Specific Heat of an Ultracold Bose Gas in a Harmonic Trap

Damaz de Jong

Supervisors: Peter van der Straten, Alexander Groot and Pieter Bons.

June 24, 2013

Abstract

In this thesis we look at theory and experiments with the purpose of finding an experimental value for the specific heat of a Bose-Einstein condensate. First, we consider basic thermodynamics in a harmonic trap to define the concept of specific heat in this context. A model is constructed for the measurements and the measurements themselves are discussed. The first part of this thesis considers a time dependent magnetic trap to add energy to the system. We will predict this increase in energy by theory to be able to calculate the specific heat. This method turns out to be impractical and difficult to implement correctly experimentally. This is partly because of experimental difficulties but mainly because the process is not sufficiently understood. The second part concerns a laser beam illuminating the cloud to induce heating like in phase contrast imaging. Although theoretical predictions and experiments do not agree with one another, a scheme is laid out to be able to determine the specific heat from these experiments.

Contents

1 Introduction

1.1 Bose-Einstein condensation

The history of Bose-Einstein condensates starts with a letter from Satyendra Nath Bose to Albert Einstein. In that letter, Bose explains a way to derive Planck's radiation formula. Einstein subsequently published a paper in 1924 describing the quantum theory of an ideal gas using the theory Bose developed. In this paper he writes that for monatomic ideal Bose gases at zero temperature, the entropy must vanish and all particles should be in the lowest energy state. This new phase of matter is now called a Bose-Einstein condensate (BEC) [1].

The easiest way to think of a BEC is to describe all particles of the Bose gas as quantum mechanical wave packets with a wavelength given by the thermal De Broglie wavelength, which is given by the formula[1]:

$$\Lambda_{\mathrm{dB}} := \sqrt{\frac{2\pi\hbar^2}{mk_{\mathrm{B}}T}}. \tag{1.1}$$

The quantum mechanical uncertainty of the position of a particle is of the order of the value of Λ_{dB}. When Λ_{dB} becomes larger than the inter-particle distance, the concept of *a particle* loses its meaning. This is because two particles cannot be distinguished in any way. The system can no longer be described as a group of classical particles because quantum mechanical effects emerge on a macroscopic scale. Instead, one should view the system as a *coherent matter wave*.

The average inter-particle distance is $n^{-1/3}$, where n represents the density. For dilute gasses, n is about $10^{20}\mathrm{m}^{-3}$ [2] and in order to get a Λ_{db} that is larger than the inter-particle distance, extremely low temperatures are necessary (in the nanokelvin regime). For a long time this made it impossible for experimentalists to create a BEC. So although this new state of matter was already predicted in 1924, the first experimental observation of a gaseous BEC occurred more than 70 years later. In 1995, BEC was realized for the first time by Cornell and Wieman. Several months later, Ketterle also managed to create a BEC [3]. In 2001 Cornell, Wiemann and Ketterle were awarded the Nobel Prize in Physics [4].

The condensates are made by trapping a cloud of atoms and cooling the system down. To achieve this, both laser cooling and evaporative cooling are used. These two cooling techniques are both vital for reaching the temperature necessary for Bose-Einstein condensation.

The temperature for which a BEC starts to form in the cloud of atoms is called the critical temperature, T_{c}. For temperatures lower than this T_{c}, some particles are in the condensate while other particles are in the *thermal cloud*. However, the system cannot be treated as two separate parts. For example, the temperature is only defined for the system as a whole and not for the condensate by itself because all particles of the condensate are in the ground state.

These properties feel very counter-intuitive. To get a better understanding, it helps to have a good analogy. To this end, we consider glass. When glass melts, there is a temperature range for which the *solid* and *liquid* phase coexist. This can be compared to the coexistence of the thermal cloud and the BEC.

[1] In this equation, T stands for the temperature and m, k_{B} and $\hbar$ are constants whose values are given in appendix A.

The temperature of glass is obviously different from that of the BEC. The temperature in the analogy where glass is a solid should be thought of as $T = 0\,\mathrm{K}$ in the Bose gas and the temperature where all the glass has melted as $T = T_c$. One similarity is that the two phases of the glass are spatially mixed, just as the thermal cloud and BEC. Another is that the two phases are in thermal equilibrium. If particles are removed from one of the two phases, the remaining particles and the energy will be redistributed over the whole system. The analogy should not be driven too far, of course. The BEC is a quantum mechanical system while the glass is not, but this analogy can help develop an understanding of the BEC systems.

In the current BEC experiments, it is possible to measure the temperature of the cloud of atoms with an accuracy sufficient for quantitative analysis. This is why, for instance, the condensate fraction versus temperature has been studied experimentally [5]. On the other hand, there is no experimental value of the specific heat of a system with a BEC. This is because measurements involving the energy have not been successful in providing a quantitative result [6].

The main goal of this thesis is measuring the specific heat of the cloud containing a BEC. Since the condensate has no temperature by itself, there is no specific heat of a BEC. One should view the specific heat of a system with a BEC as the relation between the total energy and the temperature of the system. This thesis gives a model and compares it to experiments. During these experiments, it became apparent that not all effects playing a significant role are taken into account. Because of this, the results of this thesis also have an impact on a range of future experiments in the Utrecht group that are performed on BEC's. The two most important examples of this are firstly the results concerning the behaviour of a BEC in a time dependent harmonic trap and secondly the effects of phase contrast imaging (PCI) on the BEC.

The main subjects of this thesis are the description of experiments and the explanation of the corresponding theory. The experiments that we have done had the aim of measuring the heat capacity of a system with a BEC. The theory is required to get an understanding to what is happening and to be able to draw conclusions from the measurements.

The experimental setup that is used to do the experiments in this thesis is described in chapter 2. All theoretical considerations are combined in chapter 3. In chapters 4 and 5 the measurements and results are discussed of two different methods which were explored in order to determine the specific heat.

This thesis also contains an appendix which is attached after the conclusion (chapter 6). The first section gives the values of some physical constants and parameters of the experiment. Another section of the appendix is a reference for some notations that are used in this thesis and finally, the last part of the appendix gives some proofs of statements made in the main chapters.

2 Experimental Setup

2.1 Overview

Figure 1 shows an schematic overview of the experiment denoting all of the separate components.

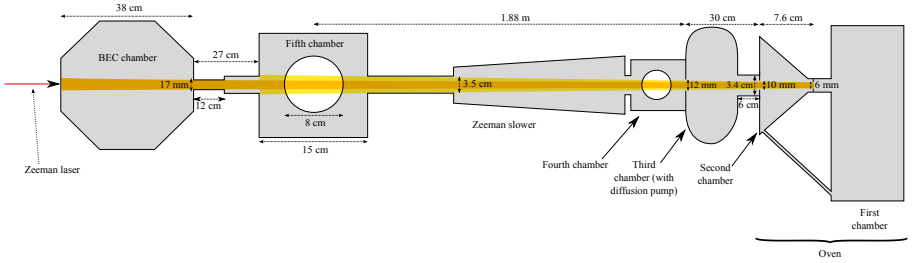

Figure 1: A schematic representation of the experiment setup. Used with permission [7].

Starting from the right, the atoms that will form the condensate originate from an oven with a temperature of about 600 K. Using two small diaphragms, a collimated beam of particles is formed. The so called *Zeeman slower* slows the beam down from a starting speed of $800\,\mathrm{m\,s^{-1}}$ to roughly $30\,\mathrm{m\,s^{-1}}$. This is achieved by a laser beam propagating in the direction opposite to the flux of particles. The frequency of the laser is resonant with the atoms such that the atoms absorb and re-emit the light, thereby losing momentum. In order for this to work, the laser has to be resonant with the atoms and due to the Doppler effect, the frequency of the laser changes in the reference frame of the atoms. The solution is to make use of the Zeeman effect. This effect is the shift of the energy levels as a function of the magnetic field. By using a decreasing magnetic field, the energy levels from the atoms can be tuned to match the frequency of the laser for each velocity [2, p. 58].

Next, the particles enter the magneto-optical trap (MOT) in the BEC chamber. In this trap the atoms are cooled further by a combination of laser light and a magnetic field. The magnetic field together with laser beams ensure a restoring force thus trapping the atoms. The laser beams also provide a force opposing the velocity of the atoms, slowing them down. The setup consists of six lasers such that for each of the three orthogonal axes there are two laser beams, one coming from the positive and one from the negative direction. Laser light which is slightly detuned to the red, relative to the cooling transition, is used[2]. When atoms are moving they are pushed in the opposite direction by the laser beam, since the beam they are moving to is closer to resonance than the beam they are moving away from due to the Doppler effect.

The cloud is now cold enough to be captured in a magnetic trap in which the final stage of the cooling process takes place. Atoms are trapped in a magnetic field by the interaction of their spin with the magnetic field. Depending on the direction of their magnetic moment relative to the magnetic field, they will

[2]This means that the laser light has a lower frequency than the resonance frequency of the cooling transition.

either move to a high or a low magnetic field (high-field and low-field seekers respectively) or will be unaffected by the field. Particles that are unaffected cannot be trapped by a magnetic trap. Furthermore, it is not possible to create a magnetic field which has a local maximum in a position, where there is no electrical current [2, p. 60]. This means that in every magnetic trap, only the low-field seekers are trapped. To increase the efficiency of loading the atoms from the MOT to the magnetic field, the atoms are optically pumped to the low-field seeking state. This process has a typical efficiency of 60 %.

The cooling works by continuously removing the atoms with the highest energy from the trap. This is done slow enough so that the system stays in thermal equilibrium. This means that only the atoms from the tail of the Boltzmann distribution are ejected and the bulk of the particles becomes cooler. Ejecting the particles is done by a radio frequency field which induces a spin-flip on the particles with a certain energy. This works because the resonance frequency for a spin-flip depends on the magnetic field. The particles with a high energy can reach parts of the trapping potential that other particles cannot reach. These parts correspond to a certain magnetic field and by choosing a frequency for the RF field that is resonant for particles in this magnetic field, the spin-flip is induced only on these particles. The frequency is ramped down until the atoms become cold enough to form a BEC. This way of cooling is called forced evaporative cooling.

The whole setup is placed in a ultra-high vacuum to prevent the BEC being destroyed by particles at room temperature moving through the condensate. Our experiment uses several vacuum pumps, including a cryogenic pump which turns out to be very important to get a pressure low enough for a BEC.

2.2 Magnetic trap

This experimental setup uses a cloverleaf trap[5] to generate the magnetic trap. The trapping potential of this trap is harmonic. An anisotropic harmonic trap can be characterised by the trap frequencies in three orthogonal directions. We denote these frequencies by ω_1, ω_2 and ω_3. These frequencies can be put in a vector $\vec{\omega} = (\omega_1 \quad \omega_2 \quad \omega_3)^{\mathrm{T}}$.

The trap in this experiment has one so called *axial* and two *radial* directions (call them respectively $\hat{\omega}_1$, $\hat{\omega}_2$ and $\hat{\omega}_3$), which are all mutually orthogonal. The axial direction is defined by the geometry of the magnetic trap, but the other two are only defined up to a rotation along the axial axis. Following the normal right-handed orientation of a coordinate system we take $\hat{\omega}_1 \times \hat{\omega}_2 = \hat{\omega}_3$.

The trap frequencies are controlled by specifying the current through the coils of the trap. This means that, in order to know the trap frequencies, they have to be measured because calculating the trap frequencies from the current is far from trivial. To measure the trap frequencies, a cloud in the magnetic trap is produced and given a kick using one of the available coils. The cloud will then obtain a dipole oscillation around the center of the trap and we make images of the cloud using PCI with a known time between two pictures. This should be enough the determine the trap frequencies, but unfortunately, in our case the imaging frequency is of the same order as the trap frequency in the radial direction.

The result of this inadequate sampling frequency is that the fitting of the dipole oscillation becomes difficult. The result of the fitting procedure can

be increased if we use the beat frequency between the trap frequency and the imaging frequency. The position r_j of the j^{th} measured point is given by

$$r_j = a_0 + a_1 \sin(\omega\tau j + \delta), \tag{2.1}$$

with τ the time between two pictures. Here a_0, a_1 and δ are three extra fit parameters to determine the offset, amplitude and phase of the oscillation. With some standard trigonometric equations, it can be written as

$$r_j = a_0 + a_1 \cos\left(\frac{2\pi}{x\tau}\tau j\right) \sin(\omega_{\text{b}}\tau j + \delta), \tag{2.2}$$

with the beat frequency $\omega_{\text{b}} = \omega - \frac{2\pi}{x\tau}$ and x an undetermined variable. Fitting with this model gives much better results, with the only problem that remains the fact that is x can have multiple values. This problem can be resolved by using two separate measurements with two different values for τ. The initial parameter for ω_{b} is taken as $\tilde{\omega}_{\text{b}} = \tilde{\omega} - \frac{\pi}{\tau}$. If $\tilde{\omega}$ is close to the actual trap frequency it turns out that $x = 2$. The measurement with a different τ can then be used to check that $\tilde{\omega}$ is sufficiently close to the trap frequency.

The process of determining the trap frequencies needs two steps. First the positions of the clouds are determined by a fitting procedure (see section 2.3) and then equation 2.2 is fitted to these positions. This process needs human supervision at this point. The reason for this lies in the analysis of the images of the cloud. The fitting procedure will not be able to find a position for the cloud if for example the cloud has moved from the imaging frame. This results in outliers in the data. As it turns out, all these outliers are caused by fits that obviously do not correspond to the image as can be checked manually. To circumvent the necessity of checking the fits by hand, we use another method. The mean and standard deviation of the positions are calculated. Then all points which lie farther than 3 standard deviations from the mean are removed from the data set. This procedure is repeated until it does no longer filter any data points from the set. This margin of 3 standard deviations turns out to remove only the points resulting from a wrong fit caused by the reasons above. This method works well, because in most cases it does not remove any data points. In the cases that remain, one or two data points are removed from the set. Equation 2.2 can then be fitted to the data. With this method, the trap frequencies can by determined fully automatically.

2.3 Imaging

We have two different ways of making images of the cloud. These are *absorption imaging* and *phase contrast imaging*. With the first method a shadow is cast by the atoms on the CCD camera with a resonant laser beam. For dense clouds the cloud becomes opaque to the laser and the resulting shadow cannot be used for a qualitative analysis due to a poor signal to noise ratio. One solution for this is to release the cloud from the magnetic trap letting it expand during several milliseconds before making the picture. Absorption imaging is destructive because the laser beam is resonant with the atoms. This means that if a series of pictures is needed to follow the dynamics of the system, a new cloud is needed for each picture. This makes absorption imaging very sensitive to run-to-run

differences of the cloud apart from the fact that this is a very time consuming method.

In phase contrast imaging (PCI) the real part of the index of refraction is measured instead of the imaginary part (the absorption). This method of imaging is less affected by the limitations of absorption imaging. It works by using a probe beam which is detuned from the resonant frequency[3] and propagates through the cloud. The refracted part of the beam is imaged by two lenses on the CCD camera. The non-refracted part of the beam is first focused on a phase spot such that this part of the beam accumulates an extra phase, which depends on the phase spot. In this experiment the light through the phase spot accumulates $5\pi/3$ less phase than the other part of the beam which is equivalent to an extra phase of $\pi/3$ [3].

A schematic representation of the PCI setup can be seen in figure 2. From geometrical optics it is found that the magnification factor of both the probe beam and the cloud is equal to $M = f_2/f_1 = 3$. Note that this factor is independent of the distance d between the two lenses. In this experimental setup, the magnification factor is determined to be $M = 3.05(5)$ [3].

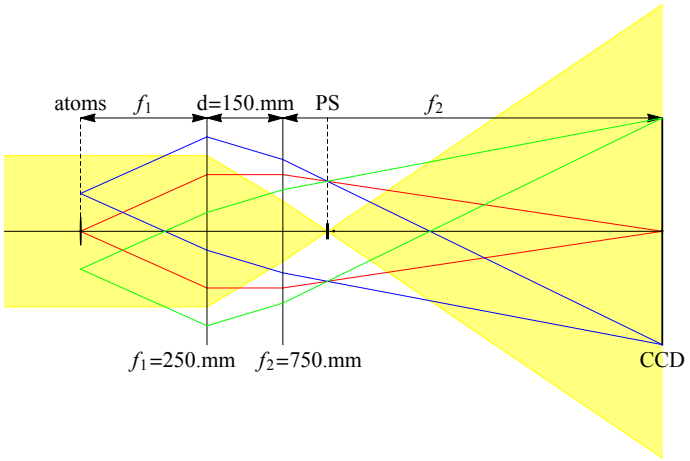

Figure 2: Schematic representation of a part of the PCI setup with the probe beam (in yellow) and three propagating beams from the atoms (in red, green and blue). The phase spot denoted by PS.

In order to get a picture of the cloud, three images are captured by the CCD camera. The first image is the laser beam shining through the atoms, the second image is taken after the atoms are gone and is a picture of the laser beam on the camera. The third image is the background image with no laser beam. These images are processed to one image ro reduce noise. The process used combines these three pictures and uses singular value decomposition to reduce the noise. For an accurate description of this process, see [8].

The next step is to extract the relevant data from the images. There are multiple ways of fitting which can be used. The easiest one is to fit a Thomas-Fermi profile [2] for the condensate and simultaneously a Gauss profile for the thermal cloud. The Thomas-Fermi approximation is far from the best model

[3]Relative to the $(F = 1)$ to $(F' = 1)$ transition.

available, but the advantages of our implementation are that it is a simple method that does not assume that the cloud is in thermal equilibrium and it does not need information about the magnetic trap in order the fit the data. This makes the model ideal for measuring the trap frequencies, where by nature of the experiment the trap frequencies are not known. The fact that there are better approximations here is irrelevant because only the coordinates of the condensate are used for which the Thomas-Fermi method is as good as any other method.

Another procedure which can be used, fits a Hartree-Fock [2] model to the data. This model is a far better approximation because it takes the interactions between the condensate and the thermal cloud into account. Our implementation of this method gives more useful data to work with than our implication of the Thomas-Fermi method. The parameters returned are the temperature and the chemical potential. In addition, the Hartree-Fock model can also give the number of particles, total energy and other thermodynamic variables. In order for our implementation to work however, the cloud must be in equilibrium. To reduce the number of fit parameters, the trap frequencies and the coordinates are usually held fixed during the fitting procedure. However, in order for this to work, the values for these parameters must be known. To find these parameters, the Thomas-Fermi model is used.

3 Theory

3.1 Thermodynamics

In a standard treatment of thermodynamics the first law of thermodynamics is stated as

$$\mathrm{d}U = đQ + đW \tag{3.1}$$

to equate the change in energy dU to an amount of heat added to the system $đQ$ and an amount of work done on the system $đW$ [9]. In this equation it holds that

$$đQ = T\mathrm{d}S, \tag{3.2}$$

where S is the entropy. The work done on the system is then often given in terms of the volume V and the pressure p:

$$đW = -p\mathrm{d}V. \tag{3.3}$$

However, in our experiment the system is contained in a harmonic trap for which there is no volume. Instead, the work done on the system is given by a change in the trap frequencies.

Following reference [10] we define two new thermodynamic quantities. The first is a substitute for the volume and will be called the *harmonic volume* $\mathcal{V}$, which is defined in terms of the trap frequencies ω_j:

$$\mathcal{V} = \bar{\omega}^{-3}. \tag{3.4}$$

The second is a substitute for the pressure and will be called the *harmonic pressure* denoted by $\mathcal{P}$. Note that the dimension of the harmonic volume is different from the dimension of the normal volume. The normal volume has the dimension L^3 while the harmonic volume has the dimension T^3. Analogously, the dimension of harmonic pressure is different from that of the normal pressure. This does not matter as long as the harmonic pressure is the conjugate of the harmonic volume such that the dimension of $\mathcal{P} \cdot \mathcal{V}$ is energy, or in SI symbols $\mathsf{L}^2\mathsf{M}\mathsf{T}^{-2}$.

This is a motivation to write

$$\mathrm{d}U = T\mathrm{d}S - \mathcal{P}\mathrm{d}\mathcal{V}. \tag{3.5}$$

We restrict ourselves here to a system of non-interacting bosons. The grand potential is defined as $\Phi_\mathrm{G} := -k_\mathrm{B}T\ln(\mathcal{Z})$. Using the quantum statistics of bosons, a formula for the grand partition function $\mathcal{Z}$ can be obtained in terms of the chemical potential μ and $\beta = 1/(k_\mathrm{B}T)$[9, p. 351]:

$$\ln(\mathcal{Z}) = -\sum_i \ln(1 - e^{\beta(\mu - E_i)}). \tag{3.6}$$

In this formula, E_i denotes the energy of the i^{th} energy level. We convert the sum to an integral and substitute the density of states[4] $g(E)$.

$$\Phi_\mathrm{G} = \frac{1}{\beta}\int_0^\infty \ln(1 - e^{-\beta(E-\mu)})g(E)\mathrm{d}E, \tag{3.7}$$

[4]Changing the sum to an integral can lead to problems if the ground state is macroscopically occupied. In this case, the contribution to the grand potential of the ground state is zero because its energy is zero.

with the density of states of a harmonic trap given by

$$g(E) = \frac{E^2 s}{2\hbar^3 \omega_1 \omega_2 \omega_3}. \tag{3.8}$$

In this formula, s is a factor to take into account the different spin states of the bosons. In the experiment, only one spin state is trapped and therefore $s = 1$ in this case.

The integral that remains can be solved using a standard formula[9, p. 471] and it is given by

$$\Phi_{\mathrm{G}} = \frac{-(k_{\mathrm{B}}T)^4}{\hbar^3 \bar{\omega}^3} \mathrm{Li}_4(z) \tag{3.9}$$

with the fugacity $z := e^{\beta\mu}$. The polylogarithm $\mathrm{Li}_n(z)$ is defined as

$$\mathrm{Li}_n(z) := \sum_{k=1}^{\infty} \frac{z^k}{k^n}. \tag{3.10}$$

Using the normal thermodynamic relation $\mathcal{P} = -\partial_{\mathcal{V}} \Phi_{\mathrm{G}}$, we obtain

$$\mathcal{P} = \frac{(k_{\mathrm{B}}T)^4}{\hbar^3} \mathrm{Li}_4(z). \tag{3.11}$$

And with equation 3.11 we find $\Phi_{\mathrm{G}} = -\mathcal{P}\mathcal{V}$.

The energy of the condensate can be written in terms of Φ_{G} as $U = -3\Phi_{\mathrm{G}} = 3\mathcal{P}\mathcal{V}$ (see appendix C.1). The specific heat is defined as

$$C_{\mathcal{V}} = \left(\frac{\partial U}{\partial T} \right)_{\mathcal{V},N}. \tag{3.12}$$

In order to be able to calculate the specific heat, the quantities that remain constant must be known. In this case these are the harmonic volume and the number of particles. Let us introduce the dimensionless variable $\chi := \frac{(k_{\mathrm{B}}T)^3}{\hbar^3 \bar{\omega}^3}$. The number of particles can be calculated with the relation $N = -\partial_\mu \Phi_{\mathrm{G}}$ which yields (see equation C.8)

$$N = \chi \mathrm{Li}_3(z). \tag{3.13}$$

After some calculations the following expression for $C_{\mathcal{V}}$ can be derived (for the derivation, see proof C.2),

$$C_{\mathcal{V}} = 3k_{\mathrm{B}} \left[4\chi \mathrm{Li}_4(\mathrm{Li}_3^{-1}(N\chi^{-1})) - \frac{3\chi^{-1}N}{\mathrm{Li}_2(\mathrm{Li}_3^{-1}(N\chi^{-1}))} \right]. \tag{3.14}$$

In this formula Li_n^{-1} denotes the inverse of a polylogarithm. This formula is not very useful because of the normal and inverse use of the polylogarithms. However, the formula can be simplified by looking at the high temperature limit. In this limit $N\chi^{-1}$ goes to zero and this means that $\mathrm{Li}_4(\mathrm{Li}_3^{-1}(N\chi^{-1}))$ and $\mathrm{Li}_2(\mathrm{Li}_3^{-1}(N\chi^{-1}))$ can be approximated by $N\chi^{-1}$. Substituting this into equation 3.14 yields

$$C_{\mathcal{V}} \approx 3k_{\mathrm{B}}(N-3) \approx 3Nk_{\mathrm{B}}. \tag{3.15}$$

This equation looks like the heat capacity of an ideal gas in a constant volume ($C_V = \frac{3}{2}Nk_{\mathrm{B}}$). The extra factor of 2 is due to the fact that we are considering a system in a harmonic trap and not in a fixed volume.

3.2 Condensed Phase

Let the wave function ψ of the condensed state with N particles be normalized to N. That is:

$$\int |\psi(\vec{r})|^2 \mathrm{d}\vec{r} = N. \tag{3.16}$$

The energy of a BEC is the sum of the internal energy, the potential energy and the kinetic energy [2]:

$$E(\psi) = \int \left[\frac{\hbar^2}{2m} |\nabla\psi(\vec{r})|^2 + V(\vec{r})|\psi(\vec{r})|^2 + \frac{1}{2} U_0 |\psi(\vec{r})|^4 \right] \mathrm{d}\vec{r}. \tag{3.17}$$

In this equation U_0 is used for the effective contact interaction and is defined by

$$U_0 = \frac{4\pi\hbar^2 a}{m}, \tag{3.18}$$

with a the scattering length (see appendix A). By minimizing equation (3.17) the Gross-Pitaevskii equation can be obtained,

$$-\frac{\hbar^2}{2m}\nabla^2\psi(\vec{r}) + V(\vec{r})\psi(\vec{r}) + U_0|\psi(\vec{r})|^2\psi(\vec{r}) = \lambda\psi(\vec{r}). \tag{3.19}$$

The λ appears as a Lagrange multiplier to keep the number of particles N constant. For a Lagrange multiplier, the following equation holds [11]:

$$\lambda = \frac{\partial E}{\partial N}. \tag{3.20}$$

We recognize the right-hand side of this equation as the thermodynamical equation for the chemical potential, so we can conclude that λ denotes the chemical potential μ. An approximation for the wave function of the BEC in a time independent trap can be found by neglecting the kinetic energy in the Gross-Pitaevskii equation.

$$|\psi(\vec{r})|^2 = \begin{cases} \frac{\mu_{\mathrm{TF}} - U(\vec{r})}{U_0} & \text{if } \mu \geq U(\vec{r}) \\ 0 & \text{if } \mu \leq U(\vec{r}) \end{cases} \tag{3.21}$$

A subscript is added to the μ to show that we are working within the Thomas-Fermi approximation.

In this thesis only a harmonic potential is considered, which is given by

$$U(\vec{r}, t) = \frac{1}{2}\sum_{j=1}^{3} m\omega_j^2 r_j^2, \tag{3.22}$$

with ω_j the angular trap frequency in the j direction. The size R_j of the condensate in the j direction is given by

$$R_j = \sqrt{\frac{2\mu}{m\omega_j^2}}. \tag{3.23}$$

The chemical potential μ can be calculated by using the normalization of ψ. It turns out that (see proof C.4)

$$\mu_{\mathrm{TF}} = \frac{1}{2}\hbar\bar{\omega}\left(15Na\sqrt{\frac{m\bar{\omega}}{\hbar}}\right)^{2/5}. \tag{3.24}$$

Combining equations (3.23) and (3.24) a formula for the number of particles in the condensed state can be found:

$$N = \frac{m^2\bar{\omega}^2\bar{R}^5}{15a\hbar^2}.$$

3.3 Selfsimilar Expansion

When we consider a BEC in a time dependent trap, the formula for the potential is given by equation (3.22) with time dependent frequencies ω_j. Due to this time dependence, the BEC will scale in the three directions with a scaling factor λ_j, where λ_j satisfies [12]

$$\ddot{\lambda}_j(t) = \frac{\omega_j^2(t_0)}{\lambda_j(t)\lambda_1(t)\lambda_2(t)\lambda_3(t)} - \omega_j^2(t)\lambda_j(t), \tag{3.25}$$

with the boundary conditions:

$$\lambda_j(t_0) = 1 \text{ and } \dot{\lambda}_j(t_0) = 0 \text{ for all } j \in \{1,2,3\}. \tag{3.26}$$

By numerically solving this coupled second order differential equation we can calculate the behaviour of the BEC in the trap.

3.4 Energy considerations

With these λ_j, the time dependent wave function of the condensate can be described. Starting with equation (3.21) and performing the scaling, this formula turns into (see proof C.3)

$$|\psi(\vec{r},t)|^2 = \frac{\mu_{\mathrm{TF}}(t_0) - U(\{r_j/\lambda_j(t)\}_{j=1,2,3}, t_0)}{U_0\lambda_1(t)\lambda_2(t)\lambda_3(t)}. \tag{3.27}$$

Note that in general, the chemical potential is a function of time because the trap frequencies ω_j are time-dependent. However, in equation 3.27 only the chemical potential at t_0 appears. The internal energy is given by (see proof C.5)

$$E_{\mathrm{int}}^{t_0}(t) := \int \frac{1}{2}U_0|\psi(\vec{r})|^4 \mathrm{d}\vec{r} = \frac{2N\mu_{\mathrm{TF}}(t_0)}{7\lambda_1(t)\lambda_2(t)\lambda_3(t)}. \tag{3.28}$$

The potential energy is given by (see proof C.6)

$$E_{\mathrm{pot}}^{t_0}(t) = \frac{N\mu_{\mathrm{TF}}(t_0)}{7}\sum_{j=1}^{3}\gamma_j^2\lambda_j^2(t), \tag{3.29}$$

with $\gamma_j(t) := \omega_j(t)/\omega_j(t_0)$. The ground state energy of a BEC at t_0 is given by

$$E_{\mathrm{ground}}(t_0) = E_{\mathrm{int}}^{t_0}(t_0) + E_{\mathrm{pot}}^{t_0}(t_0) = \frac{5N\mu_{\mathrm{TF}}(t_0)}{7}. \tag{3.30}$$

To calculate $E_{\mathrm{kin}}^{t_0}$ we first approximate the trap frequencies as a piecewise constant function with jumps at t_i with $i \in \mathbb{N}$. Then the energy of the BEC is conserved in the time interval (t_{i-1}, t_i) and we denote this energy by E_i. Then $E_i =$

$E^{t_0}_{\text{pot}}(t^+_{i-1})+E^{t_0}_{\text{int}}(t^+_{i-1})+E^{t_0}_{\text{kin}}(t^+_{i-1})$ and also $E_i = E^{t_0}_{\text{pot}}(t^-_i)+E^{t_0}_{\text{int}}(t^-_i)+E^{t_0}_{\text{kin}}(t^-_i)$. But $E^{t_0}_{\text{int}}$ and $E^{t_0}_{\text{kin}}$ are continuous so we can drop the limit in these two functions. By the Thomas-Fermi approximation, $E^{t_0}_{\text{kin}}(t_0) = 0$. Let $\Delta P^{t_0}(t_i) := E^{t_0}_{\text{pot}}(t^+_i) - E^{t_0}_{\text{pot}}(t^-_i)$ and we get

$$\begin{aligned} E^{t_0}_{\text{kin}}(t_i) =& E^{t_0}_{\text{kin}}(t_{i-1}) + E^{t_0}_{\text{int}}(t_{i-1}) - E^{t_0}_{\text{int}}(t_i) + E^{t_0}_{\text{pot}}(t^+_{i-1}) - E^{t_0}_{\text{pot}}(t^+_i) + \Delta P^{t_0}(t_i) \\ =& E^{t_0}_{\text{int}}(t_0) - E^{t_0}_{\text{int}}(t_i) + E^{t_0}_{\text{pot}}(t^+_0) - E^{t_0}_{\text{pot}}(t^+_i) + \sum_{j=1}^{i} \Delta P^{t_0}(t_i). \end{aligned} \tag{3.31}$$

It is now possible to calculate the energy added to the system by the time dependent magnetic trap.

$$E_{\text{trans}} = E^{t_{\text{s}}}_{\text{pot}}(t_{\text{f}}) + E^{t_{\text{s}}}_{\text{int}}(t_{\text{f}}) + E^{t_{\text{s}}}_{\text{kin}}(t_{\text{f}}) - E_{\text{ground}}(t_{\text{f}}). \tag{3.32}$$

In this whole section, the influence of gravity has been ignored. Gravity certainly has an impact on the system because when the trap frequencies are lowered, the cloud will drop. This will induce a dipole mode in the system but the energy which is stored in a dipole mode cannot thermalize in a harmonic trap. All dipole modes can be ignored, and therefore, the gravity can be left out of the equations.[6, 13]

3.5 Scattering

When the laser beam illuminates the cloud, some atoms will scatter to excited states. The excited atoms will then fall back to one of the ground states. Some of the ground states are trapped whereas others are not. In this section we will make a theoretical model to describe this process.

The chance that an atom will scatter by the laser light is expressed by the so called scatter rate Γ_{sc} [14].

$$\Gamma_{\text{sc}} = -\frac{1}{\hbar\epsilon_0 c}\text{Im}(\alpha(\beta))I. \tag{3.33}$$

In this equation, c is the speed of light and ϵ_0 is the vacuum permittivity. The values for these constants can be found in appendix A. The intensity of the laser is denoted by I and $\alpha(\beta)$ is the angle between the polarization of the light and the quantization axis. For π-polarized light, $\beta = 0$ and for a linear combination of σ^+- and σ^--polarized light, $\beta = \pi/2$.

The initial state of the atoms in the cloud is the $(F = 1, M_F = -1)$ state. From the $(F = 1, M_F = -1)$ state, there are three possible transitions, namely to the $F = 0$, $F = 1$ and $F = 2$ state and the M-state depends on the polarization of the light. These three transitions each have a different resonance frequency and a different transitions strength. Let the detuning of transition e with the laser be denoted by δ_e and the transition strength by $\mathcal{D}_e(\beta)$. The polarizability can be calculated and it is given by [3]:

$$\alpha(\beta) = \frac{3i\epsilon_0\lambda^3}{4\pi^2}\sum_e \frac{\mathcal{D}_{F_e}(\beta)}{1 - 2i\delta_e/\gamma} \tag{3.34}$$

where $\lambda = 2\pi c/\omega$ is the wavelength of the laser, $\gamma = \tau^{-1}$ is 1 over the lifetime τ of the excited states. The transition strengths are given by:

$$\begin{aligned}\mathcal{D}_0(\beta) =& \frac{4}{24}\sin^2(\beta)\\ \mathcal{D}_1(\beta) =& \frac{5}{24}(1+\cos^2(\beta))\\ \mathcal{D}_2(\beta) =& \frac{1}{24}(6+\sin^2(\beta))\end{aligned} \tag{3.35}$$

We see that the scattering rate Γ_{sc} has a contribution from each of the three transitions. This is a motivation to define a scattering rate Γ^e_{sc} per transition:

$$\Gamma^e_{\text{sc}} = -\frac{1}{\hbar\epsilon_0 c}\text{Im}\left(\frac{3i\epsilon_0\lambda^3}{4\pi^2}\frac{\mathcal{D}_{F_e}(\beta)}{1-2i\delta_e/\gamma}\right) I. \tag{3.36}$$

Note that $\Gamma_{\text{sc}} = \sum_e \Gamma^e_{\text{sc}}$. The probability distribution over the ground states of the particle can be described with a vector. There are eight ground states, three for $F = 1$ and five for $F = 2$. We can now write all the probabilities as a vector in the $\mathbb{R}^3 \bigoplus \mathbb{R}^5$. The same can be done for the excited states of which there are nine (ignore the seven $F = 3$ excited states because the atoms cannot scatter to the $F = 3$ state). These nine probabilities can be written as a vector in the $\mathbb{R}^1 \bigoplus \mathbb{R}^3 \bigoplus \mathbb{R}^5$.

Consider one atom in the $(F = 1, M_F = -1)$ state. When the laser beam illuminates a particle, there is a chance that the particle will scatter to an excited state. To prevent getting needlessly long equations, consider the most important case of π-polarized light, i.e. $\beta = 0$. The probability vector of the excited states can then be calculated. In the scattering event with linear polarized light, the magnetic quantum number M_F does not change. The vector therefore becomes:

$$\phi_{\text{E}} = t_{\text{exp}} \begin{pmatrix} 0 & \Gamma^1_{\text{sc}} & 0 & 0 & \Gamma^2_{\text{sc}} & 0 & 0 & 0 & 0 \end{pmatrix}^{\text{T}}, \tag{3.37}$$

with t_{exp} the duration of the laser pulse. In all experiments considered in this thesis, $t_{\text{exp}} \gg \tau$ From these excited states, the atoms will fall back to a ground state due to spontaneous emission of a photon. Using the branching ratios from reference [15, p. 285] the probabilities of decaying to a certain ground states are known. This decay can be conveniently written down as a matrix. Split the decay in three parts, one for each of the polarization directions of an emitted photon. These matrices act on the excited probability vectors and sends them to a probability vector of the ground states. With these matrices we can write the probability distribution of a particle that has scattered to the excited state and decayed back to the ground state as

$$\phi_{\text{G}} = (\mathcal{S}_{\sigma^-} + \mathcal{S}_{\sigma^+} + \mathcal{S}_{\pi}) \cdot \phi_{\text{E}}. \tag{3.38}$$

The explicit form of the matrices $\mathcal{S}_{\sigma^-}$, $\mathcal{S}_{\sigma^+}$ and $\mathcal{S}_{\pi}$ is given below together with a fourth matrix $\mathcal{T}$. This matrix is defined on the probability vectors of the ground states to be able to exclude any states that are not trapped by the magnetic field. For $F = 1$, only the state with a negative magnetic quantum number is trapped while for $F = 2$ the states with a positive magnetic quantum number are trapped. This is due to the fact that the gyromagnetic factor for $F = 1$ and $F = 2$ has an opposite sign.

$$\mathcal{S}_{\sigma^-} = \frac{1}{60}\begin{pmatrix} 0 & 0 & 20 & 0 & 0 & 0 & 0 & 0 \\ 0 & 25 & 0 & 0 & 0 & 1 & 0 & 0 \\ 0 & 0 & 25 & 0 & 0 & 0 & 3 & 0 \\ 0 & 0 & 0 & 0 & 0 & 0 & 0 & 6 \\ 30 & 0 & 0 & 0 & 10 & 0 & 0 & 0 \\ 0 & 15 & 0 & 0 & 0 & 15 & 0 & 0 \\ 0 & 0 & 5 & 0 & 0 & 0 & 15 & 0 \\ 0 & 0 & 0 & 0 & 0 & 0 & 0 & 10 \\ 0 & 0 & 0 & 0 & 0 & 0 & 0 & 0 \end{pmatrix} \qquad \mathcal{S}_{\pi} = \frac{1}{60}\begin{pmatrix} 0 & 25 & 0 & 0 & 0 & 15 & 0 & 0 & 0 \\ 20 & 0 & 0 & 0 & 0 & 0 & 20 & 0 & 0 \\ 0 & 0 & 0 & 25 & 0 & 0 & 0 & 15 & 0 \\ 0 & 0 & 0 & 0 & 20 & 0 & 0 & 0 & 0 \\ 0 & 3 & 0 & 0 & 0 & 5 & 0 & 0 & 0 \\ 0 & 0 & 4 & 0 & 0 & 0 & 0 & 0 & 0 \\ 0 & 0 & 0 & 3 & 0 & 0 & 0 & 5 & 0 \\ 0 & 0 & 0 & 0 & 0 & 0 & 0 & 0 & 20 \end{pmatrix}$$

$$\mathcal{S}_{\sigma^+} = \frac{1}{60}\begin{pmatrix} 20 & 0 & 0 & 0 & 0 & 0 & 0 & 0 & 0 \\ 0 & 0 & 0 & 6 & 0 & 0 & 0 & 0 & 0 \\ 25 & 0 & 0 & 0 & 3 & 0 & 0 & 0 & 0 \\ 0 & 25 & 0 & 0 & 0 & 1 & 0 & 0 & 0 \\ 0 & 0 & 0 & 0 & 0 & 0 & 0 & 0 & 0 \\ 0 & 0 & 0 & 10 & 0 & 0 & 0 & 0 & 0 \\ 5 & 0 & 0 & 0 & 15 & 0 & 0 & 0 & 0 \\ 0 & 15 & 0 & 0 & 0 & 15 & 0 & 0 & 0 \\ 0 & 0 & 30 & 0 & 0 & 0 & 10 & 0 & 0 \end{pmatrix} \qquad \mathcal{T} = \begin{pmatrix} 1 & 0 & 0 & 0 & 0 & 0 & 0 & 0 & 0 \\ 0 & 0 & 0 & 0 & 0 & 0 & 0 & 0 & 0 \\ 0 & 0 & 0 & 0 & 0 & 0 & 0 & 0 & 0 \\ 0 & 0 & 0 & 0 & 0 & 0 & 0 & 0 & 0 \\ 0 & 0 & 0 & 0 & 0 & 0 & 0 & 0 & 0 \\ 0 & 0 & 0 & 0 & 0 & 0 & 0 & 0 & 0 \\ 0 & 0 & 0 & 0 & 0 & 0 & 0 & 1 & 0 \\ 0 & 0 & 0 & 0 & 0 & 0 & 0 & 0 & 1 \end{pmatrix} \tag{3.39}$$

The number of scattered atoms that are trapped per atom in the condensate can be calculated by:

$$P(\text{scattered} \wedge \text{trapped}) = \mathbb{1}_8 \cdot \mathcal{T} \cdot \phi_{\mathrm{G}}. \tag{3.40}$$

Likewise, the same number for untrapped particles can be calculated by replacing $\mathcal{T}$ with $I_8 - \mathcal{T}$.

When the atom is excited, it absorbs a photon and when it falls back to the ground state, it emits another photon in a random direction. These 2 events both give the atom a momentum of $\hbar\omega/c$, but not in the same direction. The correct total momentum transfer $\vec{p}_{\mathrm{tot}}$ has to be calculated by an integral.

$$\begin{aligned} \vec{p}_{\mathrm{tot}} &= \frac{\hbar\omega\hat{z}}{c}\frac{1}{4\pi}\int_{\partial\mathrm{Sphere}} |\vec{r} + \hat{z}|\,\mathrm{d}\vec{r} \\ &= \frac{\hbar\omega\hat{z}}{c}\frac{1}{4\pi}\int_0^{\pi}\int_0^{2\pi} \left|\begin{pmatrix} \sin\theta\cos\phi \\ \sin\theta\sin\phi \\ \cos\theta + 1 \end{pmatrix}\right| \sin\theta \mathrm{d}\phi\mathrm{d}\theta \\ &= \frac{\hbar\omega\hat{z}}{c}\frac{4}{3}. \end{aligned} \tag{3.41}$$

Now that the change in momentum is known, it is easy to calculate the corresponding energy transfer by $\frac{p^2}{2m}$.

If an atom falls back to a ground state with F=2, then there is a chance that it decays to the ground state with F=1 when it collides with another atom. When this happens, the energy difference (E_{21}) between the F=1 and F=2 state is added to the colliding atoms. What happens subsequently is difficult to predict. The amount of energy added to such an atom is enough to remove dozens of particles from the trap (by sticking them to the inside of the vacuum chamber). The energy can also be redistributed over remaining atoms giving rise to a significant rise in temperature.

4 Experiments with a time dependent trap

4.1 Behaviour of a BEC in a time dependent trap

When equation 3.25 is used to describe the behaviour of the BEC, the resulting solution can be compared to experiment. In the experiment we can control the current going to the coils of the magnetic trap. These currents can be measured and used to calculate the resulting trap frequency. The frequency at the start of the sequence is known and the trap frequency in the radial direction is linear with the current through the cloverleaf coils. The trap frequency in the axial direction is quadratic with the current through the pinch and bias coils [16]. The trap frequencies used in this experiment are shown in the next figure.

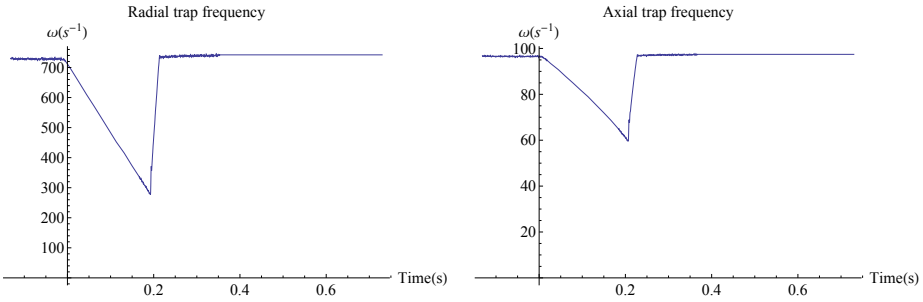

Figure 3: The radial and axial trap frequency expressed in angular frequency. This figure is the result from a calculation using the measured currents through the coils.

The initial plan to have a variation only in the axial trap frequency did not work out. The advantage of such a simple trap configuration is that the cloud does not drop due to gravity. Therefore a much smaller dipole mode is expected making imaging easier. There is also no longer any argument needed to show that the energy in the dipole mode cannot contribute to the increase in energy. Unfortunately, when this trap configuration is tried, the cloud obtains a significant velocity in the radial direction causing a non-negligible dipole oscillation. The cause of this *kick* of the cloud is probably a slight misalignment of the magnetic coils in the trap. A very small variation causes a displacement of the trap minimum, when the trap frequencies are independently changed. Therefore, a trap configuration is chosen, which changes both the axial as the radial trap frequency. Furthermore, the changes to the trap frequencies are relatively slow compared to the speed of the feedback loop controlling the currents through the coils. If a much faster change is tried, effects from the feedback loop become visible. When the feedback loop is too slow, the current through the coils overshoots. The feedback loop will subsequently lower the current resulting in a current that is below the target value. This effect results in oscillating trap frequencies, making the processing more difficult and less accurate. This is why this experiment is restricted to slower varying frequencies. The configuration of the trap is as follows: At $t = 0\,\mathrm{s}$ the cloud is decompressed during a time of 200 ms. Then there is a wait time of 1 ms followed by the compression in 20 ms. After the currents are back to their normal level, they are held constant for the

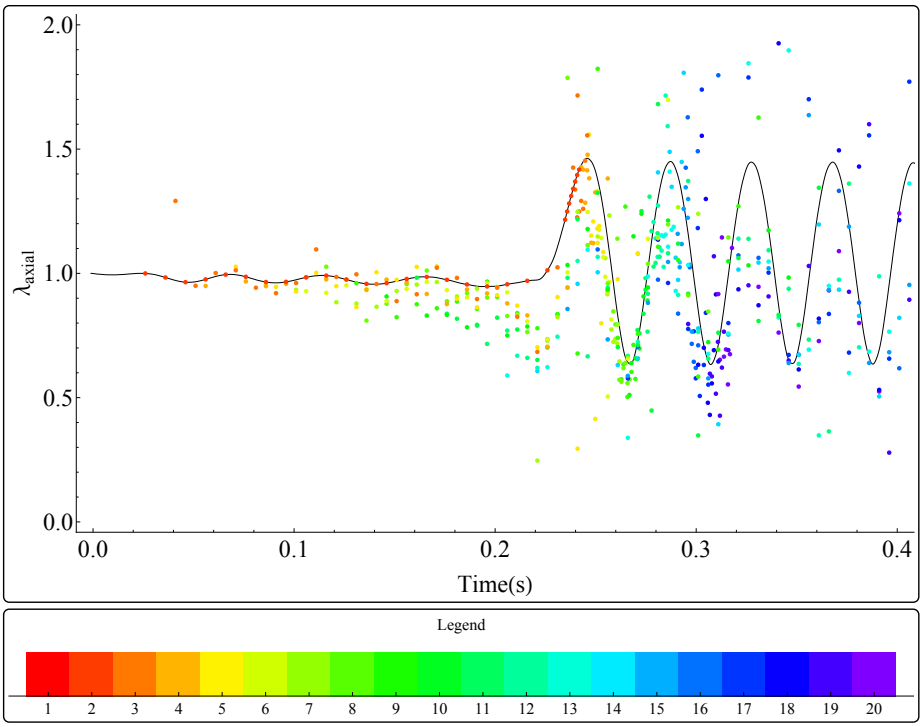

Figure 4: A plot showing the measured and predicted values of λ_{axial}. There are in total 29 data sets in this plot. The colors of the points correspond to equivalent image numbers in each dataset. This is done to be able to distinguish between clouds which have not been illuminated by the laser (red) and clouds which have been illuminated multiple times (violet).

rest of the experiment. Some noise can be seen between approximately $t = 0.2\,\mathrm{s}$ and $t = 0.4\,\mathrm{s}$ (see figure 3). After that, the currents were no longer measured but set to the level equal to the last measured value.

In order to reduce the amount of noise, a digital filter was used. This takes the mean of the surrounding values as the new measured value for each datapoint, or

$$P_j = \frac{1}{2L+1} \sum_{i=j-L}^{j+L} p_i, \tag{4.1}$$

with P_i the output, p_i the input and L the length of the filter. In this case $L = 2$ is used. The trap frequencies in the axial and the radial direction are independently measured. These two graphs have to be synchronised in time and this is done by calculating the standard deviation (σ) and the mean (μ) of the first constant piece of the graph. Then define $t = 0\,\mathrm{s}$ for the point where the graph falls below $\mu - 10\sigma$. The result is shown in figure 3.

Substituting these trapping frequencies into equation (3.25) gives a theoretical prediction for λ_j. The lambdas can be measured from the images of the condensate during the experiment. These images are made in rapid succession, for example every 5 ms. The experiment is then repeated, acquiring pictures

with a slightly different time offset to obtain a dense coverage of measurements of the radius of the condensate. The result of the axial direction is shown in figure 4. The same plot can be determined for the radial direction but then the timescales are so small that no good coverage of the oscillations can be made.

The normalized width $\lambda_j(t) = \sigma_j(t)/\sigma_j(t_0)$ is the size relative to the situation at $t = t_0$, but because this initial size is not known for the experimentally measured data, the first points per data set were multiplied such that they agreed with the predicted line. The reason that the initial size is not known is that due to experimental difficulties we cannot make images of the cloud, both before and during the adjustments of the coils and the run-to-run difference makes is impossible to use one reference image for the determination of the initial size of the cloud.

4.2 Adding energy

It is now possible to calculate the change in energy with the knowledge of the behaviour of a BEC in a time dependent trap. If in addition the starting temperature and the final temperature are known, then it is possible to create a graph of energy vs. temperature. The derivative of this graph with respect to temperature yields a value for $C_{\mathcal{V}}$.

To get a theoretical prediction, the starting temperature and number of thermal and condensed particles together with the trapping frequencies have to be used in the equations of section 3.4. The cloud that is considered here has 26 million condensed particles and 13 million particles in the thermal cloud. The starting temperature is in the order of several hundreds of nanokelvin. Equation 3.32 then yields the amount of energy added to the condensate. In this case it is 7.4 yJ. This corresponds to a rise in temperature of the order 6.9 nK which is difficult to measure.

When this is compared to experiment, the run-to-run difference makes it hard to determine the exact increase in temperature. However, analysis of the measured data indicates an increase in temperature of the order of several hundreds of nanokelvin. It becomes apparent that there is a significant effect which is not implemented in the theoretical model. Finding what extra factor is difficult because there are many effects in the cloud that could be important. For example there is a camera making images of the cloud using a laser pulse which could heat the cloud. It is difficult to see if all the energy added to the condensate has thermalized and if the cloud is in thermal equilibrium, such that the normal analyzing tools can be used. Another factor of importance is the fact that the dynamics of the thermal cloud have not been included in the theoretical model. Taking this into account could easily cause an increase of the theoretical prediction of the change in temperature.

To do this experiment correctly, for all measurements, there should be a picture of the cloud at $t = t_0$ and one after a thermalization time of 0.4 seconds or more. This turned out to be very difficult in this experiment due to how the camera is operated. The next section is devoted to exploring another method.

5 Adding energy with a laser

5.1 Theoretical prediction

In the following experiments laser pulses are used to add energy to the cloud. In this section, a theoretical prediction is calculated for these experiments by using the equations of section 3.5. The values of the parameters can be found in the appendix.

The scattering rate depends on the intensity of the laser. If we denote the number of counts per pixel of the i^{th} image of a series by $\mathcal{N}_i$, the intensity of the laser on the camera can be calculated by

$$I_{\text{cam}} = \frac{1}{q_{\text{e}} s} \frac{\mathcal{N}_i E_{\text{photon}}}{A t_{\text{exp}}}, \tag{5.1}$$

which is implicitly dependent on the frame number i. Here q_{e} and s, the quantum efficiency and the sensitivity compensate for the fact that not all photons are registered by the camera. In this experiment $q_{\text{e}} = 0.65$ and $s = 0.569$. The area of a pixel is denoted with A, which equals $8\,\mu m^2$. The exposure time is denoted by t_{exp} and E_{photon} is the energy of a photon, which is given by

$$E_{\text{photon}} = \hbar\omega = 3.37 * 10^{-19}\,\text{J}. \tag{5.2}$$

Since the image is enlarged on the camera by a factor of 3, the intensity of the beam through the cloud is 9 times as high, so $I_{\text{cloud}} = 9 I_{\text{cam}}$. The scattering rate can now be calculated from known parameters of the experiment.

The model consists of two parts. The first part is a model for the number of particles in the cloud. Every time the cloud is illuminated by the laser beam, some particles are lost from the trap. That number is proportional to the total number of particles. This model can be written as

$$N_i = N_0 (1 - g)^i, \tag{5.3}$$

where N_0 and g are undetermined parameters and i counts the number of pictures. The second part models the amount of energy added to the cloud each shot. This will be proportional to the number of atoms and to an unknown energy E_{pp}. The particles that are lost from the trap also have to be accounted for. This means that the energy of a certain frame equals the energy left from the previous frame after the removal of the lost particles plus the energy added by the laser. The amount of energy E_i in the cloud becomes

$$E_i = \frac{E_{i-1}}{N_{i-1}} N_i + N_i E_{\text{pp}} \tag{5.4}$$

which can be simplified by introducing the energy per particle $\mathcal{E}_i := E_i / N_i$. The equation then becomes (with $\mathcal{E}_0$ and E_{pp} the undetermined variables)

$$\mathcal{E}_i = \mathcal{E}_{i-1} + E_{\text{pp}} = \mathcal{E}_0 + i E_{\text{pp}}. \tag{5.5}$$

Here a prediction is made for the amount of particles lost and the amount of heating due to the laser beam. Only π-polarized light is considered as this is the polarization most used in our experiments. And one of our experiments shows

that the polarization of the light does not influence the effect on the cloud (see figure 9).

The prediction is made that an untrapped $F = 2$ particle will not decay to an $F = 1$ particle, which is a reasonable assumption because these particles will vanish from the cloud because they are not trapped. For π-polarized light, no trapped $F = 2$ atoms are created. This means that no model is needed to describe the decay of $F = 2$ particles to the $F = 1$ state. Use equation 3.38 to find that

$$g = \mathbb{1}_8 \cdot (I_8 - \mathcal{T}) \cdot \phi_{\mathrm{G}} \tag{5.6}$$

and

$$E_{\mathrm{pp}} = \frac{p_{\mathrm{tot}}^2}{2m} \mathbb{1}_8 \cdot \mathcal{T} \cdot \phi_{\mathrm{G}} \tag{5.7}$$

However, before we can get a theoretical prediction we must fix the value for the detuning of the laser. The detuning is measured with respect to the $F = 1$ to $F' = 1$ transition. If we denote the frequency of this transition by f, then the frequency of the transition to $F' = 0$ is $f - 15.8\,\mathrm{MHz}$ and the frequency of the transition to $F' = 2$ is $f + 34.3\,\mathrm{MHz}$. This means that if the laser has a detuning δ with respect to f, the following equation holds (compare with equation 3.36):

$$(\delta_0 \quad \delta_1 \quad \delta_2) = (\delta + 15.8\,\mathrm{MHz} \quad \delta \quad \delta - 34.3\,\mathrm{MHz}) \tag{5.8}$$

In this experiment, the detuning used for the laser is $\delta = -4 \times 86.5\,\mathrm{MHz}$. This enables us to give a theoretical prediction:

$$\tilde{g} := (39.3\,\frac{\mathrm{m}^2}{\mathrm{J}}) I t_{\mathrm{exp}} = \mathcal{N}_i \times 5.03 \times 10^{-6} \tag{5.9}$$

and

$$\tilde{E}_{\mathrm{pp}} := (47.3\,\frac{\mathrm{m}^2}{\mathrm{J}}) I t_{\mathrm{exp}}\,\mu\mathrm{K} = \mathcal{N}_i \times 6.06\,\mathrm{pK} \tag{5.10}$$

These are values that can be compared to the experiment.

5.2 A cloud without BEC

In this experiment the cloud with a temperature above T_{c} is illuminated by a laser beam. This means that there is no BEC in this experiment. This is done to test our model for the simplest case.

The intensity of the laser and the exposure time of the thermal cloud to the laser are varied. Ten series were used to make the fits and continue with the calculations. The trap frequencies are the same for all series and measured to be $\omega_{\mathrm{ax}} = 2\pi \times 14.9\,\mathrm{Hz}$ and $\omega_{\mathrm{rad}} = 2\pi \times 93.9\,\mathrm{Hz}$. The laser is shot 100 times through the cloud. These shots are in a rapid succession of about 10 ms and the light used has π polarization. The results are shown in figure 5 and 6. The first figure gives the relative number of particles on a logarithmic scale and the second figure the temperature of the cloud.

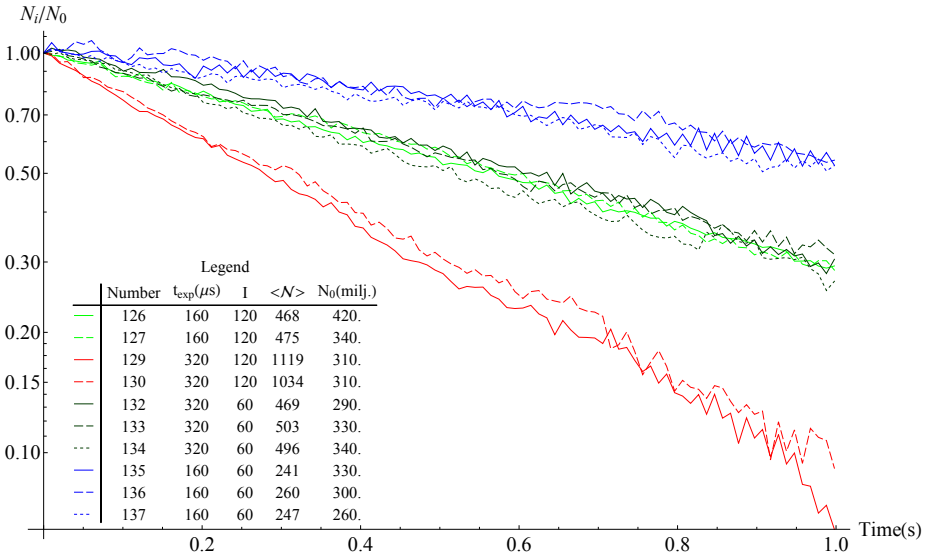

Figure 5: A plot showing the renormalized number of particles on a logarithmic scale. During the time of the experiment 100 laser pulses were fired at the cloud with a length t_{exp} and an intensity of I in arbitrary units. The number of counts per frame is listed under $< \mathcal{N} >$ and the number of particles in the first frame is listed under N_0.

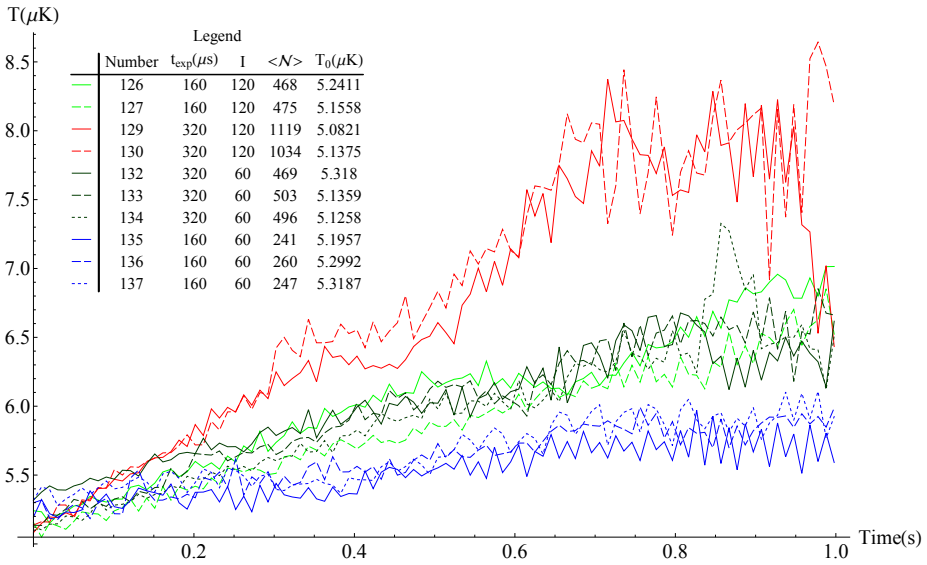

Figure 6: A plot showing the temperature of the particles in μK. These are derived from the same measurements as in figure 5. In the legend N_0 is replaced with T_0, the temperature of the cloud in the first frame.

The points in the graphs are joined to show the trend in the plots, rather than the individual measurements themselves. With the number of counts on

the camera, the model for the number of particles (see equation 5.3) can now be compared to this experiment and the fit parameter g can be determined for each series. Fitting this model to the number of particles corresponds to fitting a straight line through the data points of figure 5. The g factors can be plotted against the number of counts. The theoretical model predicts a line through the origin and the data points in figure 7.

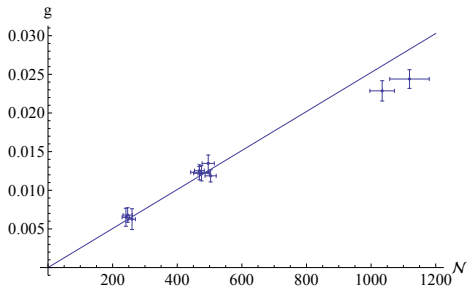

Figure 7: The experimental g factor versus the number of counts (the mean of $\mathcal{N}_i$). The error bars in the g direction have been multiplied by 10 for visibility.

The slope of the line is the relevant parameter. In figure 7 the slope is $25.2(7) \times 10^{-6}$, which is the fraction of particles lost per count on a pixel of the camera. This does not correspond to $\tilde{g}/\mathcal{N} = 5.03 \times 10^{-6}$ predicted by theory, but at least they have the same order of magnitude.

Nearly the same analysis can be performed for the energy of the cloud. The energy of the cloud can be determined by using a Hartree-Fock model and putting the found values for μ and T in the equations.

For each data series, fitting $\mathcal{E}_0$ and $E_{\rm pp}$ with equation 5.5 yields results as in figure 8a. The fits of all the series can then be plotted versus the number of counts on the camera (figure 8b).

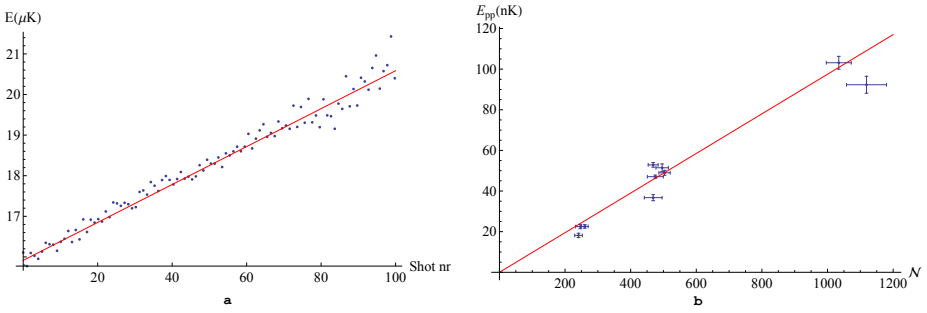

Figure 8: Left, the energy per particle of the cloud is plotted versus the time or equivalently shot number of series 127. The red line is the fit of the theoretical model. Right, the experimentally obtained $E_{\rm pp}$ are plotted versus $< \mathcal{N} >$

The slope of figure 8b is the relevant parameter that can be compared to the theory. This is the amount of energy added per particle to the cloud per count of a pixel of the camera. In this case the slope equals 97(4) pK. This is more than a factor of 10 larger than the predicted value of $\tilde{E}_{\rm pp}/\mathcal{N} = 6.06\,{\rm pK}$. A check with

formula 3.15 gives an energy increment per particle of $E_{\rm pp} = 7.3 \times 10^{-31}$ J (this is the value resulting from the fit) corresponds to a temperature increment of 17.6 nK per shot, or 1.76 µK in total. This is in good agreement with experiment. See for instance the line of number 126 in figure 6, which shows a temperature increase of about 1.77 µK. This means that that the high temperature limit gives a good description in this case (see also figure 15). Another conclusion is that the missing factor of 10 must be somewhere in the theory. The most plausible reason for the failure of the model is that the assumption is made that all particles in the $(F = 2)$ states, which are not trapped for π-polarized light, just vanish form the trap. If one of these particles will make the transition to a $(F = 1)$ state, the energy increase is large. The increase in energy per shot is in the order of tens of millikelvins if all particles in an $(F = 2)$ state fall back to an $(F = 1)$ state.

It is very difficult to predict the behaviour of particles in the $(F = 2)$ state and therefore a theoretical prediction is hard to find. However, the value for $E_{\rm pp}$ found in this experiment, uses only known facts from the system. In particular, we are allowed to use the value of $C_{\mathcal{V}}$ in the Hartree-Fock model to determine $E_{\rm pp}$. If in the next experiment, where there is a BEC in the system, the $E_{\rm pp}$ derived in this section can be used to measure the specific heat of a system containing a BEC.

5.3 A cloud with BEC

In this experiment the atoms are cooled such that there is a BEC in the system that is studied. The trap frequencies differ somewhat from the previous experiment and are determined to be $2\pi \times 15.5$ Hz in the axial direction and $2\pi \times 104.5$ Hz in the radial direction.

As in the previous section, fits can be made for the g factor and then plotted against $\mathcal{N}$ (see figure 9).

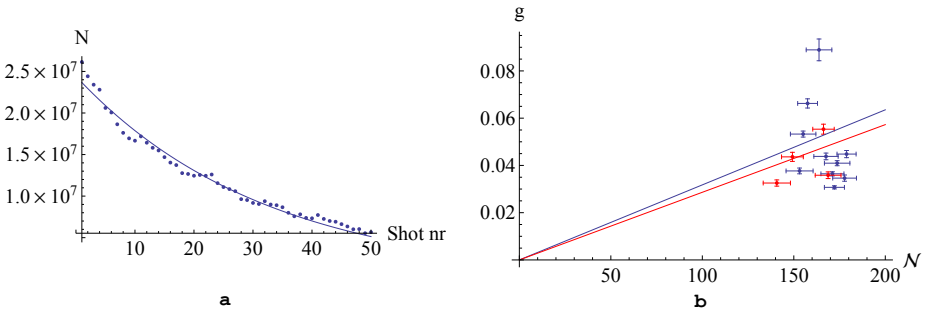

Figure 9: Left, an example of the measured exponential decay of the number of particles. Right, the experimentally obtained g factors versus $\mathcal{N}$, where the laser beam is π-polarized (blue) or σ-polarized (red).

The slopes of the two lines can be compared to theory. The data for π-polarization has a slope of $318(40) \times 10^{-6}$ and the data for σ-polarization has a slope of $286(29) \times 10^{-6}$. This indicates that the slopes are equal within their uncertainty and thus that there is no difference between π and σ polarized

light, where the g factor is concerned. Both of the slopes are different from the theoretical prediction.

This first part has been the same here as in section 5.2. Figures 10a and 10b show respectively the temperature and the total energy versus the shot number.

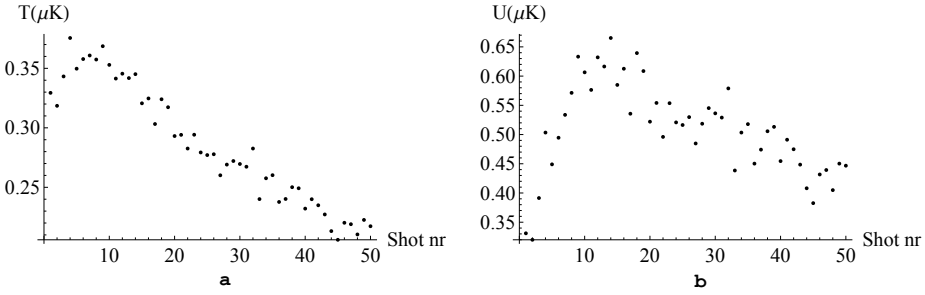

Figure 10: Left, the temperature of the cloud. Right, the energy per particle in the cloud in microkelvin.

The temperature of the cloud increases in the first 8 points but then decreases for the remaining data points. The total energy of the cloud shows the same behaviour, increasing the first 8 points and decreasing for the remaining data points. The decrease in temperature in temperature and energy is not predicted by our model. We can analyse the first 8 points similar to the analysis in section 5.2. This yields $E_{\mathrm{pp}}/\mathcal{N} = 227(8)\,\mathrm{pK}$ From this we see that this value is different from the theoretical prediction.

For the remaining data points, the laser beam cools the cloud down which is normally much more difficult than randomly illuminating it with a laser beam. The decline in temperature is not only surprising because it is not predicted by our model, but also because an earlier experiment with similar experimental conditions does not show this behaviour. The number of particles and the temperature of this experiment are plotted in figures 11 and 12.

These correspond to a g factor of 0.0123 or equivalently $g/\mathcal{N} = 162(10) \times 10^{-6}$. This value is larger than the theoretical prediction and also larger than in the measurement without a BEC in section 5.2, but is only half of the value calculated from figure 9.

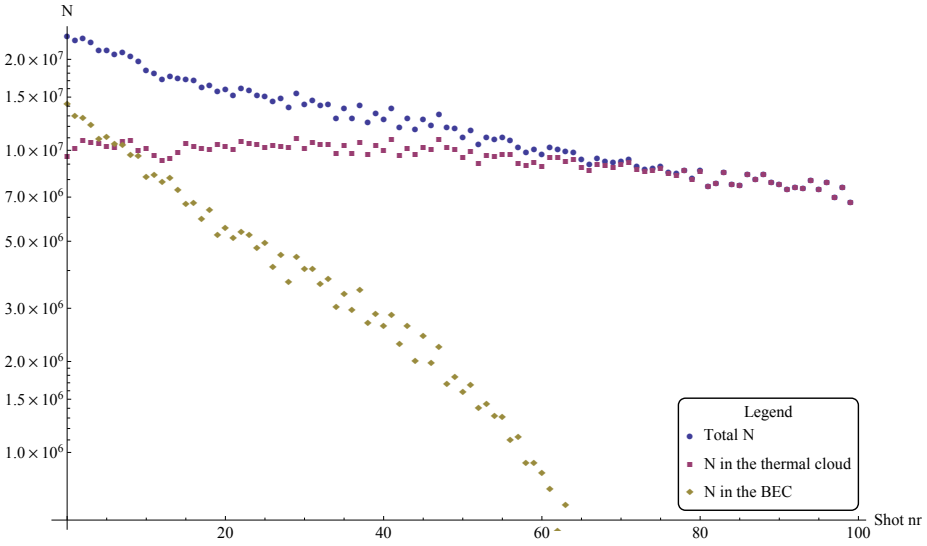

Figure 11: This plot on a logarithmic scale shows the total number of particles, combining the number of particles in the BEC and thermal cloud.

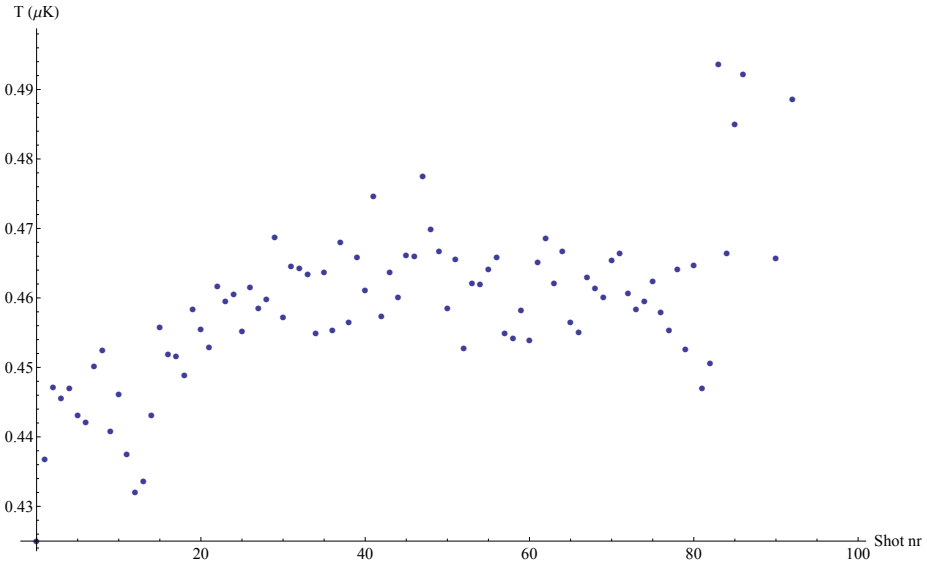

Figure 12: This graph shows the temperature of the system versus the number of shots.

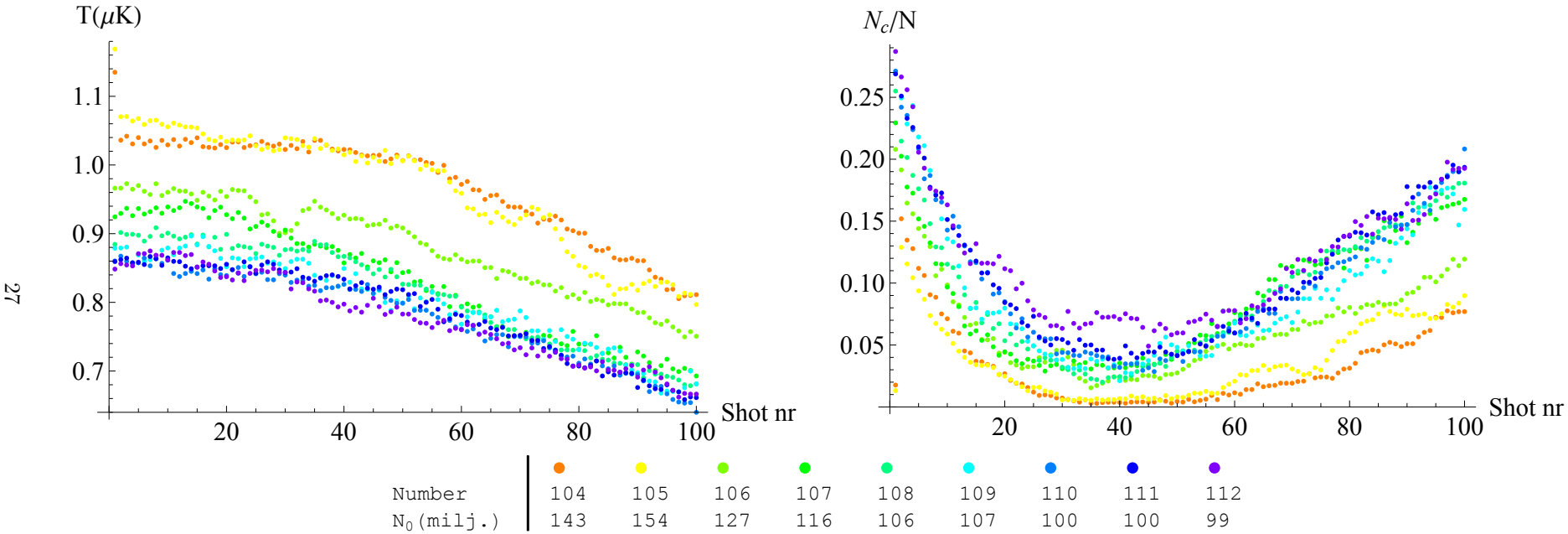

Figure 13: The temperature (left) and the condensate fraction (right) are plotted against the shot number. For each series, the number of particles in the first shot is given in the legend.

The phenomenon that the cloud seems to be cooled using a laser can be reproduced. To reproduce the cooling of the cloud, we made a series of nine condensates, each under the same experimental conditions. The results of these measurements are shown in figure 13. However looking at the raw images themselves (see figure 14) it is hard to believe that the analysis of the data is correct. Two conclusions can be drawn from these figures. The first is that the difference between two runs is high (the number of particles varies about 50%). The second significant effect is that the fitting procedure seems to find a higher μ and lower T than one would expect from figure 14. The BEC seems to have vanished in the second half of figure 14, while figure 13 seems to indicate a higher BEC fraction. The problem is not simply that the fitting procedure used to find the temperature of the cloud is stuck in a local minimum and that it can by solved by giving better starting parameters. The procedure uses the last found fitting parameters as starting parameters for the next frame and because the difference between consecutive frames is small, this results in starting parameters close to the actual minimum. When using the result of previous fits for the next fits, one has to be careful that one failed fit does not lead to a series which goes completely wrong. In the series considered here however, each fitted profile shows good correspondence with the picture.

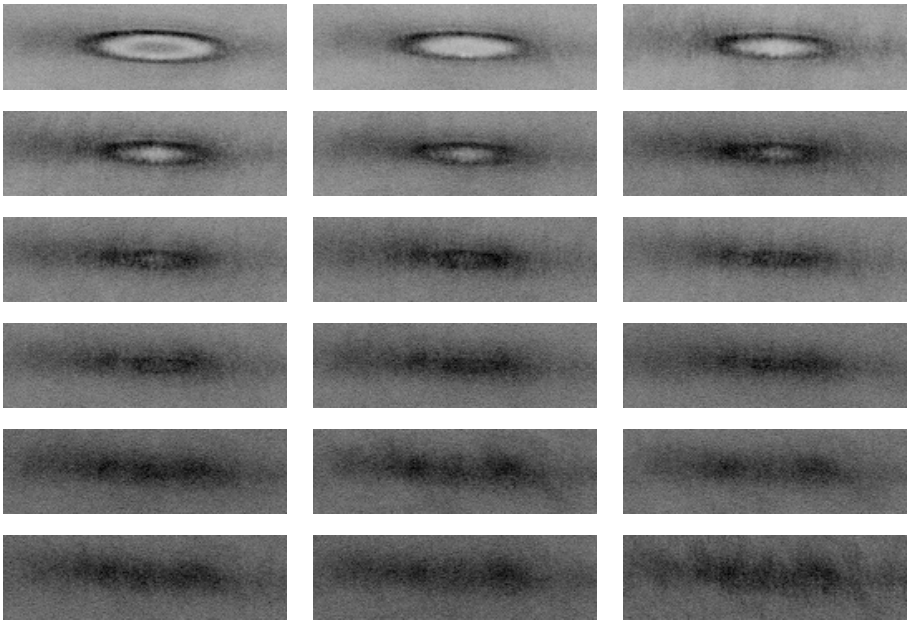

Figure 14: The original pictures of the experiment. Every fifth picture is shown to give an overview of the whole process. These are the images from Experiment 109 (compare with figure 13). The order is from left to right and from top to bottom.

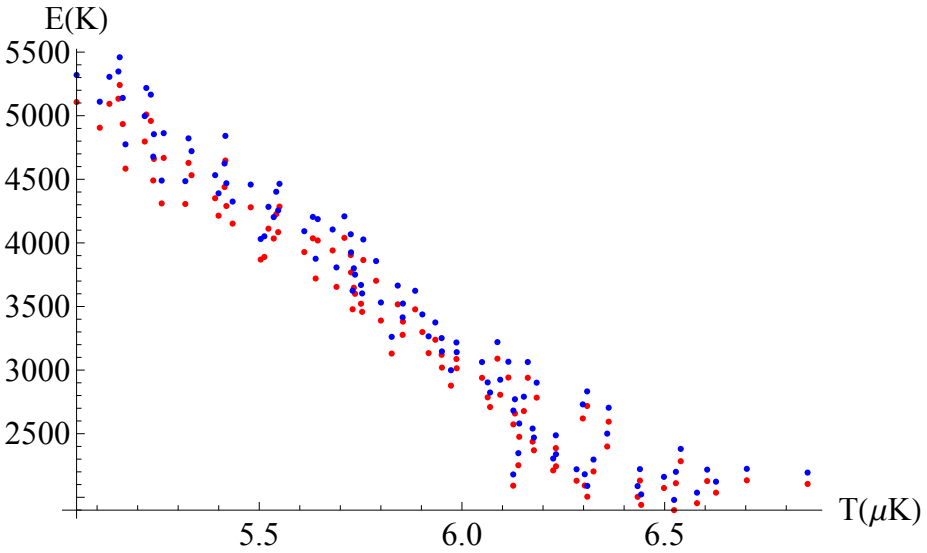

Figure 15: The points in blue were calculated form the experimental data using the Hartree-Fock model, the points in red were calculated using the high temperature limit of the heat capacity (formula 3.15). The fact that the energy seems to decrease as temperature increases is due to the fact that the number of particles is not constant but decreases as time progresses and temperature increases.

The energy of the cloud can be plotted versus the temperature. Both the temperature and the energy result from the Hartree-Fock fitting procedure. For clouds with a temperature above the critical temperature, the resulting graph is given in figure 15. The energies can be compared with the energy in the high temperature limit resulting from equation 3.15, $U = 3Nk_{\mathrm{B}}T$. The high temperature limit in figure 15 corresponds better to the data for the higher temperatures than for the lower temperatures.

For clouds containing a BEC we can compare the energy with both the high temperature limit as the energy resulting from the approximation $\mu = 0$. The resulting graph is given in figure 16. The approximation $\mu = 0$ corresponds better with the data than the high temperature limit. If the energy and temperature are determined independently, an experimental value for $C_{\mathcal{V}}$ can be obtained by taking the inverse of the derivative of the line through the data points of figure 15 and 16. However in these graphs the energy and temperature determined by the fitting procedure are not independent. The Hartree-Fock model uses a theoretical value of $C_{\mathcal{V}}$ to relate the energy to the temperature. Therefore, figure 15 and 16 can be used to get a feeling for the behaviour of the system in different regimes, but not for obtaining an experimental value for the specific heat.

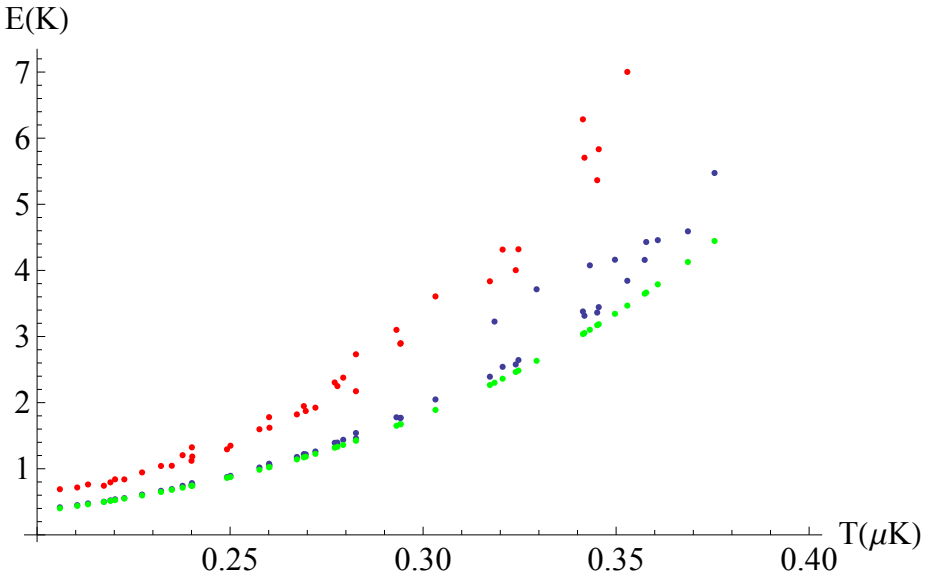

Figure 16: The points in blue were calculated using the Hartree-Fock model, the points in red were calculated using the high temperature limit of the heat capacity (formula 3.15) and the points in green were calculated using the approximation that $\mu = 0$ in equation 3.14. Note that the results of equation 3.14 are not plotted here, for these require extensive numerical integration and would not increase the insight in the specific heat of the system.

5.4 Analyzing the difference

In the experiments analyzed in sections 5.2 and 5.3 it became apparent that theory does not coincide with the experiment. In this section, some effects are examined to determine which factors are important. Effects of the fitting procedure are discussed in section 5.3 concerning the temperature of the cloud. There is another effect which may influence the quality of the fits being made. In fitting the cloud with a Hartree-Fock model, thermal equilibrium is assumed, but if the effects of shooting at the condensate bring it from thermal equilibrium and the system does not have enough time between two succeeding pulses to rethermalize, the derived values for μ and T are no longer valid. To test this, we did an experiment with different times between the pulses. In the first series a time between the pulses of $\tau = 10.1\,\text{ms}$ is used and in the second series $\tau = 100.1\,\text{ms}$ is used, leaving all other parameters fixed.

We measure $g/\tilde{g}$ to quantify the difference between the theoretical prediction and the experiment. We find that $g/\tilde{g} = 17(3)$ for $\tau = 10.1\,\text{ms}$ and $g/\tilde{g} = 16(3)$ for $\tau = 100.1\,\text{ms}$. These two values are identical within their uncertainties and therefore we conclude that the thermalization time is not a critical factor in the experiment.

For all experimental data, the relative difference between the model and the experiment $g/\tilde{g}$ can be determined and the result can be plotted against other variables. On possibility is to make a graph of the relative difference versus the chemical potential μ.

The experimental results for a wide variety of chemical potentials are given in figure 17. Because the scale of the chemical potential varies very rapidly, the μ-axis is rescaled in a non conventional way.

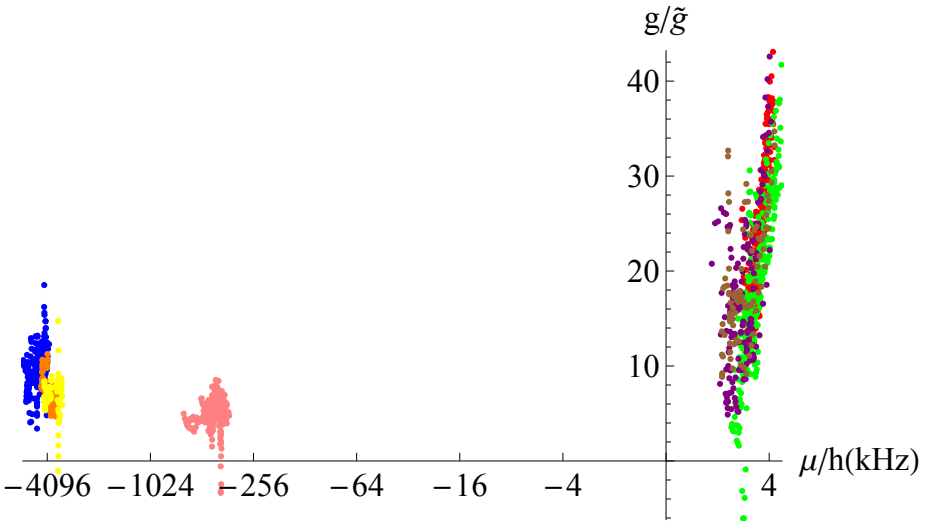

Figure 17: This plot shows the relative difference of the model and the experiment as a function of the chemical potential, Different colors represent different experimental conditions.

A theoretical ground for this relation may be in the quantum statistical effects of the atoms that influence the scattering rate, an effect that has not been taken into account. The scattering rate calculated in section 3.5 treats all atoms individually. However, in the experiment we have a cloud of atoms. When the probability of finding another atom within one wavelength λ of the atom, the scattering rate is modified.

These effects can enhance the absorption significantly. To give an idea reference [3] describes that for certain parameters this effect will increase the absorption by a factor of 3. As it is difficult to calculate a theoretical prediction for this enhancement, no comparison with figure 17 is possible. However, this will not be the only effect that causes the difference because one would expect that the relative difference goes to 1 in the high classical limit (corresponding with a large negative μ) which is not what can be seen in figure 17.

It is very difficult to get an accurate value for the g-factor because the chemical potential also changes when the laser is shot at the cloud. This results in data with a great amount of noise as can be seen form the figure. The qualitative behaviour however, can still be seen. To measure the specific heat, this enhancement factor must be understood with a greater precision and in order to do that more experiments are needed.

6 Conclusion

We have presented a model that describes the cloud in the trap but it does not take all relevant processes of the system into account. The experiments show larger effects to disturbances than theory predicts. The discrepancy between theory and experiment is large enough that the model is not applicable for finding the specific heat of a BEC.

The experiment of varying a magnetic trap to add energy to the system is very difficult to implement correctly. The measurements done in this way, described in this thesis lead to the conclusion that there are more effects playing a role than have been described by our model. Therefore the model must be expanded. The experimental difficulties, such as the run-to-run difference, must be solved as well. It can be concluded that determining the specific heat of the system by varying the trap frequencies is impractical.

Using laser excitations produces more useful results. The theory provides a prediction within the order of magnitude for a system with no BEC. The discrepancy can be solved by measuring the effects of the laser excitations on a cloud with a high temperature. Because we can describe this system fully we can use this to construct a gauge. This gauge can be used to determine the energy added to the BEC. This can then be used to measure the specific heat of a BEC. Our measurements indicate quantum enhancement of the scattering rate. This enhancement has to be taken into account to determine the specific heat and a multitude of experiments are needed to this end.

The behaviour of the cloud shows a decreasing temperature of the cloud when a laser beam illuminates the cloud. However, we do not believe this to be a physical effect, but rather an effect resulting from the fitting procedure. The mechanisms leading to this effect have to be found as this is vital information for making PCI images. In order to do this, more measurements are needed and time to analyse them. The fitting procedure has to be changed, such that it fits each image independently. When all these mechanisms are understood, getting the specific heat will probably not impose further problems.

Acknowledgements

I would like to thank my supervisor, Peter van der Straten, for presenting challenges concerning the research and giving his insight when I was stuck. This inspired me to keep working and kept the research interesting, for it was not too difficult, nor too easy. Pieter Bons and Alexander Groot also deserve my thanks. They have been very patient in explaining the fact that a BEC has no temperature over and over again. Without them, it would not have been possible to do the experiments I did, for the experimental setup is difficult to master. I would like to thank them for their time doing these experiments with me. The technical staff deserve my thanks as well. They have been very helpful in the moments that parts in the experiment broke.

Advice given by Frank de Jong has been a great help in writing this thesis. Finally, I would like to express my appreciation to Martijn van 't Woud, Peter Elroy, Johan van der Tol and Jasper Smits for discussing various topics concerning Bose-Einstein condensation. I wish to acknowledge the help provided by Johan van der Tol consisting of Hartree-Fock simulations.

Appendices

A Constants

Boltzmann Constant	k_{B}	$1.3806 \times 10^{-23}\,\mathrm{J/K}$
Speed of Light	c	$299792458\,\mathrm{m/s}$
Plank's Constant	$\hbar$	$1.05457 \times 10^{-34}\,\mathrm{J\,s}$
Vacuum permittivity	ϵ_0	$8.854 \times 10^{-12}\,\mathrm{F\,m^{-1}}$
Laser Frequency	ω	$2\pi \times 508.8\,\mathrm{THz}$
Natural line width	γ	$2\pi \times 9.8\,\mathrm{MHz}$ [17]
Detuning from $(F = 1)$ to $(F' = 1)$ transition	δ	$2\pi \times 4 \times 86.5\,\mathrm{MHz}$
Camera quantum efficiency	q_{e}	0.65
Camera sensitivity	s	0.569
Energy difference between F=1 F=2	E_{21}	$85\,\mathrm{mK}$[17]
s-wave scattering length	a	$2.804(24)\,\mathrm{nm}$[3]

B Notation

$a := b$ means that a is by definition equal to b.
a^{T} denotes the transpose of a.
đ denotes an inexact differential [9, p. 107].

$$
\begin{aligned}
(a,b) :=& \{x \in \mathbb{R} | a < x < b\} \\
< a > :=& \frac{1}{n}(a_1 + \ldots + a_n) \\
\bar{a} :=& (a_1 a_2 a_3)^{1/3} \\
\mathbb{1}_n :=& \begin{pmatrix} 1 & 1 & \ldots & 1 \end{pmatrix}^T \in \mathbb{R}^n \\
I_n =& \mathrm{diag}(1, 1, \ldots, 1) \\
\partial_x f :=& \left(\frac{\partial f}{\partial x}\right) \\
\ln(x) :=& \int_1^x \frac{1}{\xi} \mathrm{d}\xi \\
f(x^+) :=& \lim_{\xi \downarrow x, \xi \neq x} f(\xi) \\
f(x^-) :=& \lim_{\xi \uparrow x, \xi \neq x} f(\xi)
\end{aligned}
$$

C Proofs

Theorem C.1.

$$U = -3\Phi_{\mathrm{G}} \tag{C.1}$$

Proof. Introduce the dimensionless variable χ.

$$\chi := \frac{(k_{\mathrm{B}} T)^3}{\hbar^3 \bar{\omega}^3} \tag{C.2}$$

Begin with the standard thermodynamic relation:

$$U = \Phi_{\mathrm{G}} + TS + \mu N \tag{C.3}$$

With

$$\Phi_{\mathrm{G}} = \frac{-(k_{\mathrm{B}}T)^4}{\hbar^3\bar{\omega}^3}\mathrm{Li}_4(z) \tag{C.4}$$

The entropy and number of particles, S and N are derivatives of the grand potential. To calculate these derivatives, first note that for polylogarithms:

$$\partial_z \mathrm{Li}_n(z) = \partial_z \sum_{k=1}^{\infty} \frac{z^k}{k^n} = \sum_{k=1}^{\infty} \partial_z \frac{z^k}{k^n} = \sum_{k=1}^{\infty} \frac{z^{k-1}}{k^{n-1}} = \frac{\mathrm{Li}_{n-1}(z)}{z} \tag{C.5}$$

This can be used to calculate S and N.

$$S = -\partial_T \Phi_{\mathrm{G}} = 4k_{\mathrm{B}}\chi\mathrm{Li}_4(z) - k_{\mathrm{B}}T\chi\frac{\mathrm{Li}_3(z)}{z}\frac{\mu z}{k_{\mathrm{B}}T^2} \tag{C.6}$$

This leads to:

$$S = k_{\mathrm{B}}\chi\left(4\mathrm{Li}_4(z) - \frac{\mu}{k_{\mathrm{B}}T}\mathrm{Li}_3(z)\right) \tag{C.7}$$

For the number of particles N, the following equation holds:

$$N = -\partial_\mu \Phi_{\mathrm{G}} = k_{\mathrm{B}}T\chi\frac{\mathrm{Li}_3(z)}{z}\frac{z}{k_{\mathrm{B}}T} = \chi\mathrm{Li}_3(z) \tag{C.8}$$

Substituting this into equation C.3 gives:

$$U = \Phi_{\mathrm{G}} + k_{\mathrm{B}}T\chi\left(4\mathrm{Li}_4(z) - \frac{\mu}{k_{\mathrm{B}}T}\mathrm{Li}_3(z)\right) + \chi\mu\mathrm{Li}_3(z) \tag{C.9}$$

This can be simplified to:

$$U = \Phi_{\mathrm{G}} + 4k_{\mathrm{B}}T\chi\mathrm{Li}_4(z) = -3\Phi_{\mathrm{G}} \tag{C.10}$$

□

Theorem C.2.

$$C_{\mathcal{V}} = 3k_{\mathrm{B}}\left[4\chi\mathrm{Li}_4(\mathrm{Li}_3^{-1}(N\chi^{-1})) - \frac{3\chi^{-1}N}{\mathrm{Li}_2(\mathrm{Li}_3^{-1}(N\chi^{-1}))}\right] \tag{C.11}$$

Proof.

$$C_{\mathcal{V}} := (\partial_T U)_{N,\mathcal{V}} = \left(\partial_T \frac{3(k_{\mathrm{B}}T)^4}{\hbar^3\bar{\omega}^3}\mathrm{Li}_4(z)\right)_{N,\mathcal{V}} \tag{C.12}$$

The condition that N should be constant, means the μ and therefore z is not constant. In order to replace μ by N, we invert the formula for N. Denote the inverse polylogarithm by Li_n^{-1}. The dimensionless variable χ is defined in equation C.2. We can express $\mathrm{Li}_4(z)$ in terms of N in the following way:

$$\mathrm{Li}_4(z) = \mathrm{Li}_4(\mathrm{Li}_3^{-1}(N\chi^{-1})) \tag{C.13}$$

When we substitute this in the equation for the energy, we get:

$$C_{\mathcal{V}} = \left(\partial_T \frac{3(k_{\mathrm{B}}T)^4}{\hbar^3\bar{\omega}^3}\mathrm{Li}_4(\mathrm{Li}_3^{-1}(N\chi^{-1}))\right)_{N,\mathcal{V}} \tag{C.14}$$

Before we calculate the whole derivative, lets first calculate $\partial_x \mathrm{Li}_n(\mathrm{Li}_{n-1}^{-1}(x))$, (use equation C.5) we get:

$$\partial_x \mathrm{Li}_n(\mathrm{Li}_{n-1}^{-1}(x)) = \frac{\mathrm{Li}_{n-1}(\mathrm{Li}_{n-1}^{-1}(x))}{\mathrm{Li}_{n-1}^{-1}(x)}\partial_x \mathrm{Li}_{n-1}^{-1}(x) = \frac{x}{\mathrm{Li}_{n-1}^{-1}(x)}\frac{1}{\partial_y \mathrm{Li}_{n-1}(y)} \tag{C.15}$$

Where $y = \mathrm{Li}_{n-1}^{-1}(x)$, so we get:

$$\partial_x \mathrm{Li}_n(\mathrm{Li}_{n-1}^{-1}(x)) = \frac{x}{\mathrm{Li}_{n-1}^{-1}(x)}\frac{\mathrm{Li}_{n-1}^{-1}(x)}{\mathrm{Li}_{n-2}(\mathrm{Li}_{n-1}^{-1}(x))} = \frac{x}{\mathrm{Li}_{n-2}(\mathrm{Li}_{n-1}^{-1}(x))} \tag{C.16}$$

Continue with the heat capacity:

$$C_{\mathcal{V}} = \frac{12k_{\mathrm{B}}(k_{\mathrm{B}}T)^3}{\hbar^3\bar{\omega}^3}\mathrm{Li}_4(\mathrm{Li}_3^{-1}(N\chi^{-1})) + \frac{3(k_{\mathrm{B}}T)^4}{\hbar^3\bar{\omega}^3}\frac{N\chi^{-1}(-3N\frac{1}{T}\chi^{-1})}{\mathrm{Li}_2(\mathrm{Li}_3^{-1}(N\left(\frac{\hbar\bar{\omega}}{k_{\mathrm{B}}T}\right)^3))} \tag{C.17}$$

To simplify the previous equation:

$$C_{\mathcal{V}} = 3k_{\mathrm{B}}\left[4\chi\mathrm{Li}_4(\mathrm{Li}_3^{-1}(N\chi^{-1})) - \frac{3\chi^{-1}N}{\mathrm{Li}_2(\mathrm{Li}_3^{-1}(N\chi^{-1}))}\right] \tag{C.18}$$

□

Theorem C.3.

$$|\psi(\vec{r},t)|^2 = \frac{\mu_{\mathrm{TF}}(t_0) - U(\{r_j/\lambda_j(t)\}_{j=1,2,3}, t_0)}{U_0\lambda_1(t)\lambda_2(t)\lambda_3(t)} \tag{C.19}$$

Proof. Because of the selfsimilar expansion, the following must hold for every volume $V \subset \mathbb{R}^3$. Let V' be the corresponding volume at $t = t_0$ (before the expansion), so let $V' = \{L^{-1}\vec{x}|\vec{x} \in V\}$ with $L_{ij} = \delta_{ij}\lambda_i(t)$.

$$\iiint_V |\psi(\vec{r},t)|^2 \mathrm{d}\vec{r} = \iiint_{V'} |\psi(\vec{r},t_0)|^2 \mathrm{d}\vec{r} \tag{C.20}$$

Using the substitutions $x_j = \lambda_j(t)r_j$, the right hand side of the equation becomes

$$\iiint_V |\psi(\vec{r},t)|^2 \mathrm{d}\vec{r} = \iiint_V \frac{|\psi(\{x_i/\lambda_i(t)\}_{i=1,2,3}, t_0)|^2}{\lambda_1(t)\lambda_2(t)\lambda_3(t))}\mathrm{d}\vec{x} \tag{C.21}$$

Rename $\vec{x}$ to $\vec{r}$ on the right hand side, use equation 3.21 and note that, because this holds for every volume, the integrands must be equal. □

Theorem C.4.

$$\mu_{\mathrm{TF}}(t_0) = \frac{1}{2}\hbar\bar{\omega}(t_0)\left(15Na\sqrt{\frac{m\bar{\omega}(t_0)}{\hbar}}\right)^{2/5} \tag{C.22}$$

Proof. The normalization of ψ gives that $N = \iiint |\psi(\vec{r}, t_0)|^2 \mathrm{d}\vec{r}$

$$N = \iiint \frac{\mu_{\mathrm{TF}}(t_0) - \frac{1}{2}\sum_{j=1}^{3} m\omega_j^2(t_0) r_j^2/\lambda_j^2(t))}{U_0 \lambda_1(t)\lambda_2(t)\lambda_3(t)} \mathrm{d}\vec{r} \tag{C.23}$$

Where the integral is over the volume where the integrand is positive. Let $y_j = \sqrt{\frac{m}{2}}\omega_j(t_0) r_j/\lambda_j(t)$, then

$$N = \frac{1}{(\sqrt{\frac{m}{2}}\bar{\omega})^3 U_0} \iiint \left(\mu_{\mathrm{TF}}(t_0) - y_1^2 - y_2^2 - y_3^2\right) \mathrm{d}\vec{y} \tag{C.24}$$

Where the integral is still over the volume where the integrand is positive. This volume is equal to a sphere with radius $\sqrt{\mu_{\mathrm{TF}}(t_0)}$. Changing to spherical coordinates gives:

$$N = \frac{4\pi}{(\sqrt{\frac{m}{2}}\bar{\omega})^3 U_0} \int_0^{\sqrt{\mu_{\mathrm{TF}}(t_0)}} \left(\rho^2 \mu(t_0) - \rho^4\right) \mathrm{d}\rho = \frac{8\pi \mu_{\mathrm{TF}}^{5/2}(t_0)}{15(\sqrt{\frac{m}{2}}\bar{\omega})^3 U_0} \tag{C.25}$$

Solving for μ_{TF} and using that $U_0 = 4\pi\hbar^2 \frac{a}{m}$ completes the proof. □

Theorem C.5.

$$E_{\mathrm{int}}^{t_0}(t) := \int \frac{1}{2} U_0 |\psi(\vec{r})|^4 \mathrm{d}\vec{r} = \frac{2N\mu_{TF}(t_0)}{7\lambda_1(t)\lambda_2(t)\lambda_3(t)} \tag{C.26}$$

Proof.

$$E_{\mathrm{int}}^{t_0}(t) = \frac{1}{2} U_0 \int \left[\frac{\mu_{\mathrm{TF}}(t_0) - U(\{r_i/\lambda_i(t)\}_{i=1,2,3}, t_0)}{U_0 \lambda_1(t)\lambda_2(t)\lambda_3(t)}\right]^2 \mathrm{d}\vec{r} \tag{C.27}$$

Let $y_j = \sqrt{\frac{m}{2}}\omega_j(t_0) r_j/\lambda_j(t)$.

$$E_{\mathrm{int}}^{t_0}(t) = \frac{1}{2U_0 \left(\sqrt{\frac{m}{2}}\bar{\omega}\right)^3 \bar{\lambda}^3(t)} \int \left(\mu_{\mathrm{TF}}(t_0) - (y_1^2 + y_2^2 + y_3^2)\right)^2 \mathrm{d}\vec{y} \tag{C.28}$$

Change to spherical coordinates.

$$E_{\mathrm{int}}^{t_0}(t) = \frac{2\pi}{U_0 \left(\sqrt{\frac{m}{2}}\bar{\omega}\right)^3 \bar{\lambda}^3(t)} \int_0^{\sqrt{\mu_{\mathrm{TF}}(t_0)}} \left(\mu_{\mathrm{TF}}(t_0) - \rho^2\right)^2 \rho^2 \mathrm{d}\rho \tag{C.29}$$

Solving the integral gives.

$$E_{\mathrm{int}}^{t_0}(t) = \frac{8\pi \mu_{\mathrm{TF}}^{5/2}(t_0)}{15 U_0 \left(\sqrt{\frac{m}{2}}\bar{\omega}\right)^3} \frac{2\mu_{\mathrm{TF}}(t_0)}{7\lambda_1(t)\lambda_2(t)\lambda_3(t)} \tag{C.30}$$

Recognizing a factor of N (see equation (C.25)) gives:

$$E_{\mathrm{int}}^{t_0}(t) = \frac{2N\mu_{TF}(t_0)}{7\lambda_1(t)\lambda_2(t)\lambda_3(t)} \tag{C.31}$$

□

Theorem C.6.

$$E_{\text{pot}}^{t_0}(t) := \int V(\vec{r},t)|\psi(\vec{r})|^2 \mathrm{d}\vec{r} = \frac{N\mu_{TF}(t_0)}{7}\sum_{j=1}^{3}\gamma_j^2\lambda_j^2(t) \tag{C.32}$$

Proof.

$$E_{\text{pot}}^{t_0}(t) = \int \left[\frac{\mu_{\text{TF}}(t_0) - U(\{r_i/\lambda_i(t)\}_{i=1,2,3},t_0)}{U_0\lambda_1(t)\lambda_2(t)\lambda_3(t)}\right]\frac{1}{2}\sum_{j=1}^{3} m\omega_j^2(t)r_j^2\mathrm{d}\vec{r} \tag{C.33}$$

Let $y_j = \sqrt{\frac{m}{2}}\omega_j(t_0)r_j/\lambda_j(t)$.

$$E_{\text{pot}}^{t_0}(t) = \frac{1}{\sqrt{\frac{m}{2}}^3\bar{\omega}^3(t_0)U_0}\int(\mu_{\text{TF}}(t_0) - y_1^2 - y_2^2 - y_3^2)\left(\sum_{j=1}^{3}\frac{\omega_j^2(t)}{\omega_j^2(t_0)}\lambda_j^2(t)y_j^2\right)\mathrm{d}\vec{y} \tag{C.34}$$

Using equation (C.25) to remove the $\bar{\omega}(t_0)$ and interchanging the summation and the integral yields

$$E_{\text{pot}}^{t_0}(t) = \frac{15N}{8\pi}\mu_{\text{TF}}^{-5/2}(t_0)\sum_{j=1}^{3}\int(\mu_{\text{TF}}(t_0) - y_1^2 - y_2^2 - y_3^2)\frac{\omega_j^2(t)}{\omega_j^2(t_0)}\lambda_j^2(t)y_j^2\mathrm{d}\vec{y} \tag{C.35}$$

Note that $\gamma_j(t) := \omega_j(t)/\omega_j(t_0)$ and change to spherical coordinates. For each integral, choose the z-axis in the j direction such that $y_j = \rho\cos(\theta)$.

$$E_{\text{pot}}^{t_0}(t) = \frac{15N}{8\pi}\mu_{\text{TF}}^{-5/2}(t_0)\sum_{j=1}^{3}\iiint(\mu_{\text{TF}}(t_0) - \rho^2)\gamma_j^2(t)\lambda_j^2(t)\rho^2\cos^2(\theta)\rho^2\sin(\theta)\mathrm{d}\phi\mathrm{d}\theta\mathrm{d}\rho \tag{C.36}$$

Let $u = \cos(\theta)$, calculate the ϕ part and split the integral in an ρ and u part.

$$E_{\text{pot}}^{t_0}(t) = \frac{15N}{4}\mu_{\text{TF}}^{-5/2}(t_0)\sum_{j=1}^{3}\left[\gamma_j^2(t)\lambda_j^2(t)\right]\int_0^{\sqrt{\mu_{\text{TF}}(t_0)}}(\mu_{\text{TF}}(t_0)\rho^4 - \rho^6)\mathrm{d}\rho\int_{-1}^{1}u^2\mathrm{d}u \tag{C.37}$$

Calculate the integrals.

$$\begin{aligned} E_{\text{pot}}^{t_0}(t) =& \frac{15N}{4}\mu_{\text{TF}}(t_0)\sum_{j=1}^{3}\left[\gamma_j^2(t)\lambda_j^2(t)\right](\frac{1}{5} - \frac{1}{7})(\frac{2}{3}) \\ =& \frac{N\mu_{TF}(t_0)}{7}\sum_{j=1}^{3}\gamma_j^2(t)\lambda_j^2(t) \end{aligned} \tag{C.38}$$

□

D Fitting procedure

D.1 popov2d

In this section, some documentation is provided for the `popov2d.pro` `variable` argument. This section is not intended for the average reader, but rather for those needing to work with this routine.

The `popov2d` can be started with a number of arguments. The only argument covered here is the `variable` argument. The `variable` argument can be used to control which parameters should be varied in the fitting procedure. This is very useful to fix, for instance, the position. Each parameter is assigned a number j. Let $b_j \in \{0, 1\}$. If parameter j should be fixed, $b_j = 0$, if it should be varied, $b_j = 1$. The parameters with their corresponding number are in the following table:

j	parameter
0	min
1	scale
2	chemical potential
3	amplitude of phase spot
4	phase of phase spot
5	x coordinate
6	y coordinate
7	binning x-direction
8	binning y-direction

j	parameter
9	magnification
10	temperature
11	absorption
12	axial trap frequency
13	radial trap frequency
14	method
15	detuning laser
16	angle

Define the variable B as a Long (instead of an Integer), otherwise the value may overflow, leading to undesirable results.

$$B = \sum_{j=0}^{16} b_j 2^j \tag{D.1}$$

And finally call `popov2d` with the argument `variable=B`. For example, if the only parameters that should vary are the chemical potential, x coordinate, y coordinate, temperature and angle, then $B = 66660$. Then the procedure `popov2d` must be called with `variable=66660`.

D.2 Determining initial parameters

In this section a method is laid out to determine the initial parameters independent of earlier fits.

An approximation for the position of the cloud can be found by first binning the image using a two dimensional variant of equation 4.1. Then calculate the mean of every row and every column of the image to get a histogram. Determine the mean value m_x and m_y of both histograms. Then assign the lowest value of x for which the value in the histogram is larger than $\frac{1}{2}m_x$ to x_l. Analogously, assign the highest of these values of x to x_h and do the same for y_l and y_h. An approximation for the center of the cloud is then given by $\tilde{x} = \frac{x_l + x_h}{2}$ and $\tilde{y} = \frac{y_l + y_h}{2}$.

The width of the cloud can be determined using the difference between x_h and x_l. This width can be used to fit a Gaussian profile to the edge of the cloud to get an approximation of the temperature.

Finally, the number of particles can be approximated by calculating the column density using reference [3] for all pixels and summing over the pixels. From the number of particles, the chemical potential can be calculated using the Hartree-Fock model.

References

[1] A. Einstein. Quantentheorie des einatomigen idealen Gases. *Sitzungsberichte der Preussischen Akademie der Wissenschaften, Physikalisch-mathematische Klasse*, pages 261–268, July 1924.

[2] C.J Pethick and H.Smith. *Bose-Einstein Condensation in Dilute Gases*. Cambridge University Press, 2002.

[3] R. Meppelink. *Hydrodynamic excitations in a Bose-Einstein condensate*. PhD thesis, Universiteit Utrecht, 2009.

[4] W. Ketterle. When Atoms behave as waves: Bose-Einstein Condensation and the Atom Laser. Nobel Lecture, December 2001.

[5] M.-O. Mewes, M.R. Andrews, N.J. van Druten, D.M. Kurn, D.S. Durfee, and W. Ketterle. Bose-Einstein Condensation in a Tightly Confining dc Magnetic Trap. *Physical Review letters*, 77(3):416–419, July 1996.

[6] P.B. Blakie, E. Toth, and M.J. Davis. Calorimetry of Bose-Einstein condensates. *Journal of Physics B: Atomic, Molecular and Optical Physics*, 40(16), August 2007.

[7] Johan van der Tol and Martijn van 't Woud. Particle flux, slow and fast. Internal group report, 2013.

[8] Jasper Smits. Formation of Faraday patterns in cigar-shaped Bose-Einstein condensates. Bachelor Thesis, 2013.

[9] S. Blundell and K. Blundell. *Concepts in Thermal Physics*. Oxford University Press, 2006.

[10] Víctor Romero-Rochín. Equation of State of an Interacting Bose Gas Confined by a Harmonic Trap: The Role of the 'Harmonic' Pressure. *Physical Review letters*, 94(13):130601, April 2005.

[11] Hasan Karabulut. The physical meaning of Lagrange multipliers. *European Journal of Physics*, 27(4):709–718, May 2006.

[12] Y. Castin and R. Dum. Bose-Einstein Condensates in time Dependent Traps. *Physical Review letters*, 77(27):5315–5319, December 1996.

[13] John F. Dobson. Harmonic-Potential Theorem: Implications for Approximate Many-Body Theories. *Physical Review Letters*, 73(16):2244–2247, October 1994.

[14] M. Greiner. *Ultracold quantum gases in three-dimensional optical lattice potentials*. PhD thesis, 2003, Ludwig-Maximilians-universität München.

[15] Harold J. Metcalf and Peter van der Straten. *Laser cooling and trapping*. Springer, 1999.

[16] Martijn van 't Woud. Calculation of the magnetic field for a BEC trap. Diploma Thesis, Utrecht university, 2013.

[17] D.A. Steck. Sodium D Line Data. `http://steck.us/alkalidata`.